Stony Brook University

Novel Polymer Thin Film Process Using Supercritical Carbon Dioxide as an Environmentally Green Solvent

A Dissertation Presented

by

Peter Gin

to

The Graduate School

in Partial Fulfillment of the

Requirements

for the Degree of

Doctor of Philosophy

in

Materials Science and Engineering

Stony Brook University

May 2012

Stony Brook University

The Graduate School

Peter Gin

We, the dissertation committee for the above candidate for the

Doctor of Philosophy degree, hereby recommend

acceptance of this dissertation.

Tadanori Koga – Dissertation Advisor
Assistant Professor, Materials Science and Engineering

Michael Dudley - Chairperson of Defense
Professor, Materials Science and Engineering

Jonathan Sokolov – Committee Member
Professor, Materials Science and Engineering

Robert Grubbs – Committee Member
Associate Professor, Chemistry

This dissertation is accepted by the Graduate School

Charles Taber

Interim Dean of the Graduate School

Abstract of the Dissertation

Novel Polymer Thin Film Process Using Supercritical Carbon Dioxide as an Environmentally Green Solvent

by

Peter Gin

Doctor of Philosophy

in

Materials Science and Engineering

Stony Brook University

2012

We have used an assortment of characterization techniques to clarify the behavior of polymer thin films and brushes in supercritical fluids, specifically the anomalous expansion associated with the density fluctuations of a fluid. We have explored the generality of the phenomena for polymer chains in supercritical fluids. It was found that anomalous expansion of polymer chains occurs regardless of the polymer-fluid interactions. We applied these principles to modify the structure and properties of robust semicrystalline polymer thin films. By combining traditional organic solvents with the novel density fluctuating supercritical carbon dioxide process, we were able to introduce a large degree of molecular level porosity, which allowed us to tune the properties of the polymer. Lastly, we investigated the adsorption of polymer chains onto a substrate from a melt. Our findings reveal important details about the formation mechanism and equilibrium conformation of the adsorbed layer. Furthermore, we show that the adsorbed polymer has suppressed swelling behavior and dynamics due to the strong interaction with the substrate.

Dedication

To Lisa and my parents.

Table of Contents

List of Figures

List of Tables

Acknowledgments

I cannot begin to express my gratitude for my mentor and friend Tad Koga. I am continually humbled and inspired by Tad's insight, work ethic, and passion for science. Without his encouragement and trust, this work would not be possible. I am honored to be his first Ph.D. student in what is sure to be a long and successful career.

I am also thankful to Dr. Maya Endoh for her guidance through my years at Stony Brook, and Dr. Atsushi Takahara, who hosted my stay at Kyushu University. I gratefully acknowledge my defense committee, colleagues, and the staff of the Department of Materials Science, Brookhaven National Lab, and the National Institute for Standards and Technology. In particular, I would like to thank Dr. Jon Sokolov for all of his technical assistance and genius.

For their unwavering support and love, I would like to thank my parents and brother. There were many rough patches through the years, but as family we got through them together, and for that I am eternally grateful. A special debt of appreciate is owed to my grandmothers, who I too seldom thank for raising me.

Finally, to my future wife Lisa, I say "thank you". If it weren't for her love and encouragement, I would not have been able to accomplish this chapter of my life. I look forward to the exciting times ahead and our future together.

Chapter I: Introduction

1.1 Goals and objectives

At temperatures and pressures above the critical point values, a single-component fluid can have densities and solvent properties approaching those of the corresponding liquid. Fluids in this regime are defined as "supercritical fluids" (SCFs) (Fig. 1-1). SCFs have been widely utilized as regeneration solvents in a range of technical and chemical processes, such as chromatography, extraction, reactor cleanup and preparation of pharmaceutical products[1]. The unique features of SCFs are that the solvent quality of SCFs is pressure or/and temperature dependent, while the diffusion coefficient is closer to that of a gas. In addition, by varying the external parameters of temperature and pressure, one can control the interactions in the fluid environment. In particular, much attention has been focused on supercritical carbon dioxide ($scCO_2$) for polymer processing since CO_2 has a moderate critical point with T_c = 31.3 °C, P_c = 7.38 MPa and is an environmentally benign solvent.

Unfortunately, the major disadvantage of $scCO_2$ for polymer processing is that only a limited class of polymers called "CO_2-philic", such as highly fluorinated or silicone-based polymers can be dissolved in CO_2 under relatively moderate conditions (T<100°C and P<50MPa)[2]. Recently, by using neutron reflectivity, the Koga research group found that $scCO_2$ can be absorbed to a large extent in ultrathin polymer films even when the polymer's bulk miscibility with CO_2 is very poor[3-6]. This enhancement in the solubility is universal and independent of the polymer/$scCO_2$ combinations. In contrast to conventional solvents, the region of anomalous solubility is determined by the correlation length of the density fluctuations (or the cluster size) of $scCO_2$ and therefore only occurs within the first few tens of nanometers of $scCO_2$ penetration

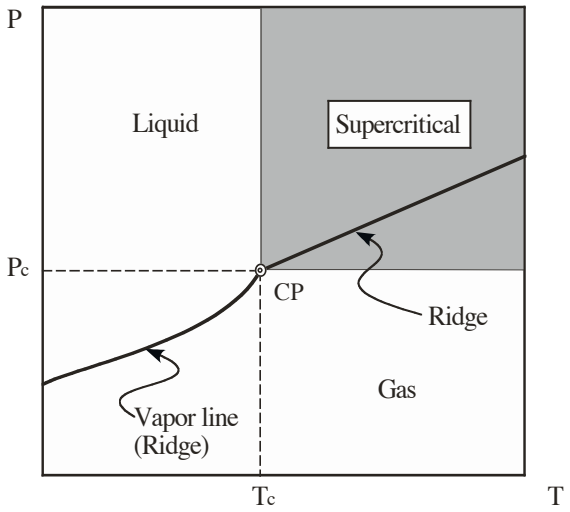

Figure 1-1. Schematic phase diagram of CO_2 near the critical point (CP).

into the polymer[3]. Consequently, it can be used very effectively to modify the surface properties of polymer films alleviating the necessity for organic solvents. The following section details of anomalous phenomena near the polymer/fluid interface.

The first object of my dissertation is to clarify the underlying physics of the density-fluctuation-induced swelling from an experimental approach. Currently, there are few theories to explain the phenomenon in the density fluctuating systems because strong, fluctuating intermolecular interactions are present. Hence, a detailed experimental description of universal principles underlying the phenomenon is crucial and will motivate theorists to tackle new physics in the understanding of the interactions between $scCO_2$ and polymers. In Chapter II, we aim to answer the following unsolved questions regarding the density-fluctuation-induced swelling:

(i) What is the underlying driving force for the swelling?

(ii) What is the role of the enthalpic interactions between the fluid and the polymer?

(iii) Is the anomalous phenomenon universal to density fluctuating fluid/polymer systems?

To achieve these goals, I have integrated a variety of *in-situ* and *real-time* x-ray/neutron scattering techniques, allowing for the formation of a comprehensive model of the interactions between the polymer and the density fluctuating SCFs and obtaining expertise in their applications to SCF/polymer systems. Moreover, in order to understand the mechanism, we introduce a simple two-state model that assumes the polymer chains belong to only two thermodynamic states (i.e., the excess swollen state and non-excess swollen state). This model along with the experimental data proposes that additional large changes in solvent-density

fluctuations around the polymer chains are accompanied with the anomalous expansion, thereby resulting in a decrease in the free energy of the entire polymer/fluid system.

The second objective of my dissertation is to establish the use of such density fluctuating supercritical fluids as new process environments or fields for polymer surface processing. In modern polymer science and technology, it is well known that various functional properties such as wettability, electrical conductivity, biocompatibility, tribology, and adhesion are governed by the surfaces and interfaces. However, the structures and properties are very difficult to understand and control. In fact, Nobel laureate Dr. Wolfgang Pauli asserted, *"God made solids, but surfaces were the work of the devil"*. Thus, in order to utilize the novel characteristics of polymeric materials, it is essential to be able to willfully manipulate surface structures and properties.

Based on the fundamental understanding of the phenomena obtained in Chapter II, I have developed a new methodology to create ultra-low dielectric (k) constant polymer films with a good metallized polymer surface to be used as the next generation of interlayer dielectric materials for microelectronics. Excluding the incorporation of fluorine to lower a material's polarity, the only alternative to achieve such low-k materials is by lowering the density of the material by introducing nanometer sized pores into initially low-k materials. As summarized in the following section, the Koga research group has already developed a simple and efficient way to introduce a large number of molecular scale pores into glassy amorphous polymer thin films utilizing density fluctuating $scCO_2$[7]. The current challenge is application towards semicrystalline polymers, which are key for meeting the stringent process and reliability requirements, such as

high thermal stability and robust mechanical properties, but at the same time are less affected by $scCO_2$ due to its crystalline structures. The studies presented in Chapter III examine the prospect of using an organic solvent, which softens semicrystalline polymers such that the penetration power of density fluctuating $scCO_2$ can be significantly enhanced, resulting in a novel and robust $scCO_2$-based process for creating ultralow-*k* semi-crystalline polymer thin films.

The third objective of my dissertation is to provide a better understanding of the formation of a very thin adsorbed polymer layer (several nanometers in thickness) at the substrate interface. The Koga group has recently shown experimental evidence of the adsorbed polymer layer, which was formed onto substrates without specific interactions of the polymer (such as π-π stacking or hydrogen bonds), having a significant influence on the viscosity distributions of ultrathin polymer films prepared on Si substrates[8]. We found that while the polymer/air interface is more mobile due to its reduced viscosity (about 30% lower than the rest of the film)[9], the long-range perturbations (~ 60 nm in thickness) associated with the adsorbed layer result in an exponential-like increase in the local viscosity with decreasing distance from the substrate interface. Although the formation of the adsorbed layer is rather general irrespective of interactions between polymers and substrates[10], little is known about the adsorption process from a melt. In Chapter IV, we provide detailed experimental descriptions of the structures and the formation process of the adsorbed polystyrene layers onto smooth, flat solids under well-controlled contacting conditions. Moreover, the swelling behavior and dynamics of the adsorbed layer in density fluctuating $scCO_2$ were studied. Another novel characteristic of density fluctuating $scCO_2$ (i.e., a screening effect on the polymer-substrate interactions) revealed that the adsorbed layer is comprised of polymer chains with two different conformations: a flattened conformation

with a larger (approximately 20%) than bulk density layer near the solid wall and a less confined, nearly random coil conformation further away from the substrate. Additional $scCO_2$ experiments on the isolated flattened layer lead to the important conclusion that the flattened conformation is thermodynamically favorable in air due to the counterbalance between the entropy loss of the polymer chains adsorbed to the substrate and the enthalpic contributions by increasing the numbers of monomer contacts with the attractive substrate. I believe that these experimental findings are a big step forward in the understanding of the structure/property relationship at the nanoscale, facilitating the development of new polymer nanostructures and nanodevices to be used in a wide variety of fields.

1.2 Significance of density fluctuating supercritical fluids for polymer surface processing

Environmentally benign supercritical fluids, such as supercritical carbon dioxide ($scCO_2$) are well regarded and studied as an alternative to conventional organic solvents used in polymer processing. CO_2 is nonflammable and nontoxic in all phases, making it considerably less harmful than solvents in its class. Organic solvents used in polymer processes are often costly to procure and difficult to dispose of, whereas CO_2 is readily available, through practices such as carbon capture, and may be released into the atmosphere or recycled after processing. Supercritical CO_2 has been shown to be a practicable, green choice for processes such as inducing self-assembly of block copolymer templates, formation of nanoporous films, and spatial implantation of nanoparticles in polymer matrices, of which are traditionally achieved using organic solvents or excess thermal energy. Supercritical fluids are known to produce annealing type effects on polymer thin films at modest conditions. The supercritical phase occurs as a result of elevated temperature and pressure above their respective critical points, as seen in Fig. 1-1, at which point

the fluid exhibits highly penetrable gas-like diffusivity characteristics coupled with liquid-like density. For CO_2, the critical temperature, Tc is 31.3 C and critical pressure, Pc is 7.38 MPa. Comparatively, the supercritical phase for CO_2 is more readily attainable than other fluids; i.e. H_2O (Tc = 374.2, Pc = 22.06). Variation in temperature and pressure of supercritical fluids enables the ability to control density dependent solvent properties. Consequently, only small manipulations are necessary to induce physical as well as thermodynamic and transport properties of the polymer. This highly tunable nature effectively makes supercritical fluids a "universal" solvent for polymers. Because of the novel features of $scCO_2$, we wish to further develop a better understanding of the processing abilities of this green solvent, especially for polymer thin films.

Good miscibility between the supercritical fluid and polymer enhances swelling effects. "CO_2-philic" polymers are known to have favorable free energies of mixing with CO_2. As a result, the compound can be dissolved in CO_2 under relatively moderate conditions ($T < 100$ °C and $P < 50$ MPa). When exposed to $scCO_2$, this class of polymer exhibits a significant degree of swelling. Unfortunately, the class of polymers that are CO_2-philic is very limited. Highly fluorinated or silicone based polymers are examples of just a hand-few of polymers that can be processed with CO_2 easily. The effectiveness of a solvent is determined by its ability to adequately dissolve one material while leaving other materials unaffected. To effectively dissolve a polymer, the solvent must overcome van der Waals forces due to intermolecular polarities in the long chained molecules. This is accomplished when both the solvent and solute are miscible with one another due to strong molecular attractions. Weak attraction to the solvent will not cause the polymer molecules to separate, as they are more attracted to each other. Solubility may be presented using numerous scales. The most applicable and commonly used

system is the Hildenbrand solubility parameter. The Hildenbrand solubility parameter ∂ is a numerical value defined as the square root of the cohesive energy density

$$\partial = \sqrt{c} = \sqrt{\frac{\Delta H - RT}{V_m}} \tag{1-1}$$

where c is the cohesive energy density, ΔH is the heat of vaporization, R is the gas constant, T is the temperature, and V_m is the molar volume. This numerical system allows for the grouping of similar solvents of comparable internal energies. Components with similar Hildenbrand solubility parameters will be attracted to one another and would be miscible. Consequently, a group of solvents with similar solubility parameters may dissolve the same polymer. Polymers which cannot be dissolved exhibit swelling behavior in precisely the same manner. The extent of swelling in polymers is greatest when the differences in the Hildenbrand values are low. Supercritical CO_2 as a solvent is not able to dissolve polymers but as a result of molecular attraction to the polymer can produce this swelling effect.

1.2.1 Introduction to density fluctuating supercritical fluids.

It is well known that SCFs are composed of inhomogeneous regions with high and low densities at the microscopic scale[11]. Near the critical point the microscopic thermal fluctuations, which occur naturally in any fluids, become strongly correlated, leading to large-scale, coherent density fluctuations[12]. The existence of the long-range density fluctuations in SCFs has been experimentally observed by partial molar volume measurements[13,14] and small-angle x-ray scattering experiments[15-17]. The density fluctuations $\langle(\Delta N)^2\rangle/\langle N\rangle$ can also be theoretically calculated from the thermodynamic relation[12],

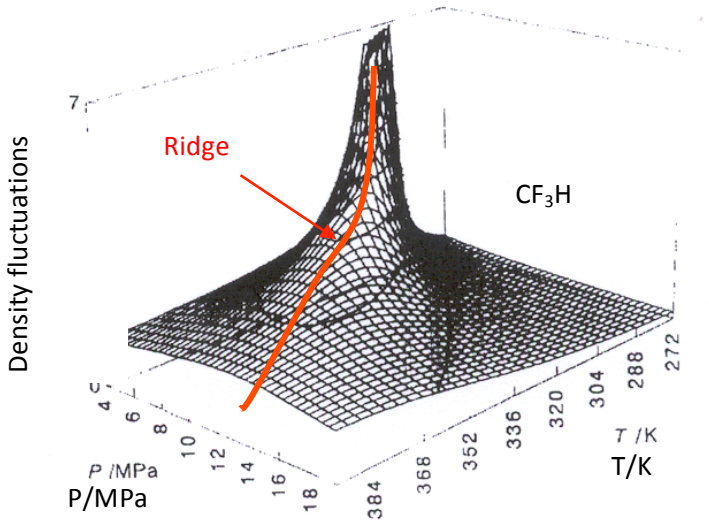

Figure 1-2. Three-dimensional density fluctuation map for CF_3H [24]. The critical point locates behind the peak.

$$\left\langle (\Delta N)^2 \right\rangle / \langle N \rangle = (N/V)\kappa_T k_B T, \qquad (1\text{-}2)$$

where N is the number of molecules in the corresponding volume V, k_B is the Boltzman constant and κ_T is the isothermal compressibility. Fig. 1-2 shows density fluctuations for CF_3H as a function of temperature and pressure[17]. The isothermal compressibility was calculated from the *P-V-T* data for the substance. From the figure one can see that the amplitude of the fluctuations shows a maximum under each isothermal condition. The locus of these maxima is known as "the density fluctuation ridge" (designated as the red line in Fig. 1-2 and the two-dimensional projection is also shown in Fig. 1-1). The ridge emanates from the critical point where the amplitude of the density fluctuations diverges and is a general feature for substances[15,17]. It is also known that the ridge corresponds to a maximum or minimum of various physical quantities such as isothermal compressibility[18], thermal conductivity[19], sound velocity[20], and partial molar volumes[13,21]. In addition, the rate constants or equilibrium constants of various chemical reactions in SCFs show maxima, minima or inflection points at the ridge[21].

1.2.2 Density-fluctuation-induced swelling of polymer thin films in $scCO_2$

Here I show the density fluctuation ridge also corresponds to the region where the solubility of CO_2 with polymer thin films achieves a maximum. Fig. 1-3 shows representative neutron reflectivity (NR) data for deuterated styrene-butadiene random copolymers (d-SBR) thin films at T = 36 °C for three different pressures. The large penetration depth inherent with neutrons makes NR an ideal tool to determine *in situ* thickness, composition, and interfacial structures of polymer thin films immersed in fluids or gases, under high pressure in thick walled vessels[5]. Deuterated polymers are essential to get high neutron scattering intensity. Specular reflectivity

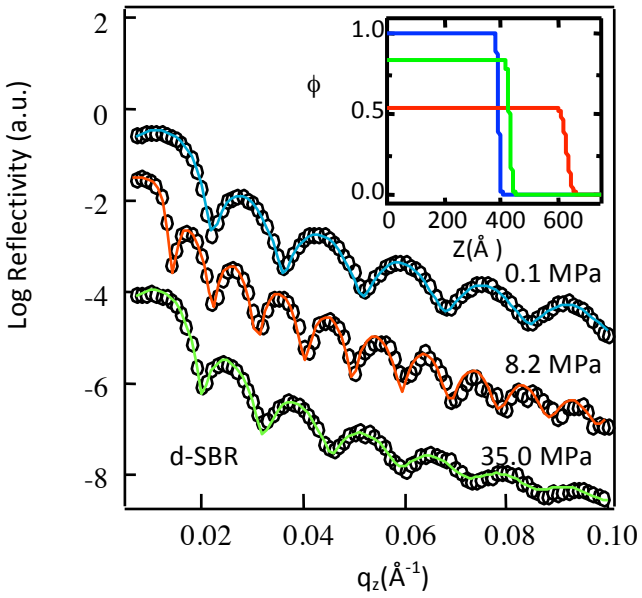

Figure 1-3. Representative reflectivity data for a d-SBR thin film at T= 36 °C. Consecutive reflectivities are shifted vertically from each other for clarity. In the inset, the d-SBR concentration (f) profiles at P = 0.1 MPa (blue line), P = 8.2 MPa (red lines) and P = 35.0 MPa (green lines) are shown.

measurements were performed on the NG7 neutron reflection spectrometer at the National Institute of Standards and Technology (NIST) with a wavelength (λ) of 4.7 Å. The data was analyzed by plotting the reflected scattering intensity as a function of the momentum transfer normal to the surface, $q_z = 4\pi \sin\theta / \lambda$, where θ is the incident angle of neutron beams. From the figure we can see that the large amplitude oscillations are observed, indicating that the surfaces are molecularly flat. The frequency of the oscillations is also seen to increase and then decrease again with pressure. The solid lines are the calculated reflectivities based on the single layer profiles[22] shown in the inset, where the values of the scattering length density are converted into the volume fractions of the polymer (f) in CO_2. The thickness of the layer, which was initially 385 Å thick, increased to 620 Å at P = 8.2 MPa, which corresponds to the ridge condition of T= 36 °C, and then decreased again to 423 Å upon compression up to P = 35.0 MPa. It should be emphasized that the dilation was an equilibrium quantity, which was a function only of the CO_2 pressure and temperature[3].

Fig. 1-4 shows the linear dilation (S_f) of the d-SBR films determined by the NR experiments. The linear dilation was calculated from the equation $S_f = (L-L_0)/L_0$, where L and L_o are the measured thickness of the swollen and unswollen polymer thin films, respectively. From the figure we can see that the large maximal values of 0.6 are observed in the dilation curves at T = 32 and 36 °C and the values of the maxima gradually decrease to approximately 0.35 with increasing temperature at T>36 °C. As the pressure is increased well into the liquid or supercritical region, i.e., P>15 MPa, the film collapses and only a small dilation of approximately 10 %, which is equivalent to the bulk swelling, is observed[5]. Upon close examination of the density fluctuations in pure CO_2 calculated by eq. (1-2), it was found that the magnitude of the excess swelling observed is strongly correlated to that of the density

fluctuations in pure CO_2, and that the anomalous maxima occur along the density fluctuation ridge (Fig. 1-4(b))[3]. Hence, in contrast to the existing concept, i.e., the density of the fluid controls the solubility of CO_2 with bulk polymers[23,24], the long-range density fluctuations can directly control the solubility of CO_2 with polymer thin films. Here are the other characteristics of the density-fluctuation-induced anomalous swelling:

a) The anomalous swelling can be scaled by the radius of polymer gyration (R_g) and is a surface effect which occurs only within ~10 R_g thickness of the polymer/CO_2 interface[3].
b) The magnitude of the anomalous swelling depends on the elasticity of the films rather than the solubility of the homopolymers with CO_2[5]. For example, the excess dilation in glassy polymers with the glass transition temperatures (T_g) of about 100 °C is at most 30%, while those in rubbery polymers exceed 60 %[3,5].
c) The anomalous swelling occurs in both spun-cast polymer thin films and polymer brushes regardless of the confinement of the chain ends[6].
d) The anomalous swelling is associated with a large decrease in T_g of the polymer thin films[4].
e) The anomalous swelling induces the excess enhancement in the interfacial width of two immiscible polymers in $scCO_2$[25].

1.2.3 Polymer surface processing using density fluctuating $scCO_2$

Moreover, when the fluid was released rapidly, the swollen structures of glassy polymer thin films could be vitrified and preserved as they were in $scCO_2$[4]. As schematically shown in Fig. 1-5, this process utilizes the vitrification of the polymer chains without formation of large additional voids, which are known to grow in the bulk when $scCO_2$ is forced under high

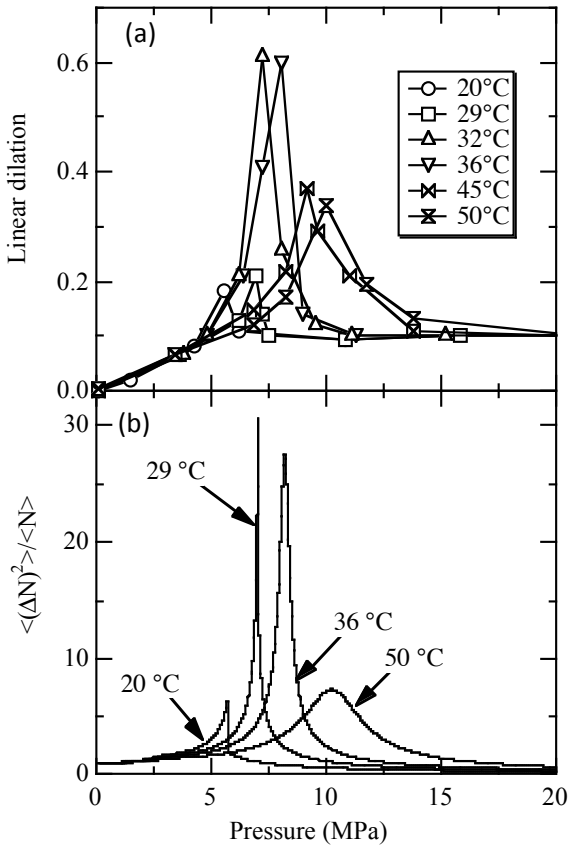

Figure 1-4. (a) Linear dilation for the d-SBR thin films as a function of pressure at different temperatures. The red line corresponds to the swelling behavior of the bulk SBR film. (b) Calculated density fluctuations of CO_2 based on the equation of state of CO_2.

pressures into immiscible polymers[26]. Detailed x-ray scattering and atomic force microscopy (AFM) experiments for the vitrified films showed no additional void structures in the length scales from 10 Å up to 100 mm. Hence this $scCO_2$ process can produce a large degree of molecular level porosity within polymer thin films[7]. The advantages of this $scCO_2$-based processing for the formation of molecular scale porosity are that (i) the porosity can be created without further processing of the polymer with corrosive solvents or heat treatments that may oxidize the polymer or damage the substrates, (ii) the film is stable as long as the temperature is below the glass transition temperature (T_g), and (iii) it is not only "environmentally-friendly" but also "polymer-friendly" because of its mild CO_2 operating conditions. The resultant films are very useful in producing coatings with low dielectric constants[7], highly gas permeable[27], and metallization properties[28].

Similar anomalous swelling of polymer thick films (1000-3000 Å) near the critical point of $scCO_2$ was reported by the Johnston and Green groups[29,30]: By using high-pressure spectroscopic ellipsometry they found that the anomalous swelling occurred in a variety of polymer films including the CO_2-philic fluorinated polymer, glassy polymers, semi-crystalline polymer, and block copolymer films. In addition, the spectroscopic data suggests an internal thick layer between the two interfacial layers, i.e., polymer/CO_2 and polymer/substrate interfaces, is responsible for the anomalous swelling[30], which is inconsistent with our x-ray reflectivity result[7].

On the other hand, Wang and Sanchez calculated the adsorption of CO_2 molecules on polymer thin films near the critical point by using a combination of the gradient theory of inhomogeneous systems and the Sanchez-Lacombe equation of state[31]. As a result, they found

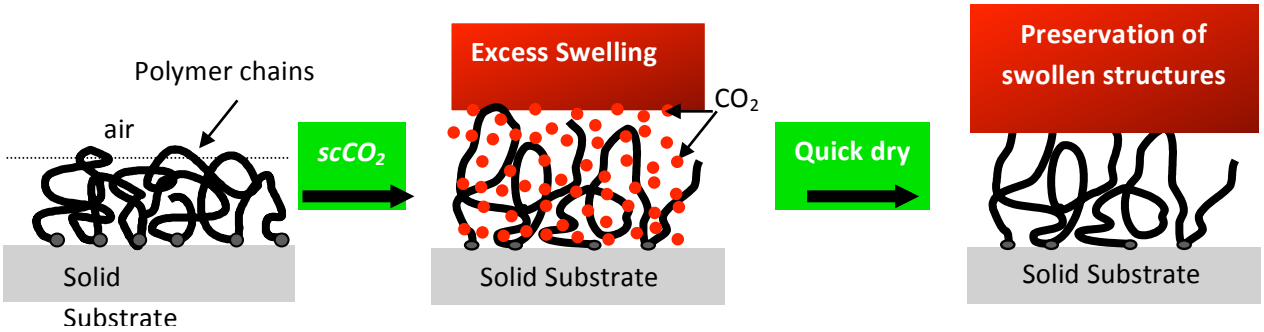

Figure 1-5. New concept for creating low-density polymer thin films using the $scCO_2$ processing.

that there was a excess adsorption layer of CO_2 molecules on the film surface and the pressure dependence of the thickness of the excess layer showed a similar maximum at the ridge to the one experimentally observed (Fig. 1-4 (a)). However, the thickness of the surface adsorption layer is estimated to be at most 30 Å, which is one order of magnitude smaller than those obtained by the NR[3-6] and ellipsometry[29,30] experiments. Hence, the mechanism of the anomalous swelling remained unclear until the experimental and theoretical study presented in Chapter II.

1.3. Polymer Brushes in density fluctuating Supercritical Carbon Dioxide

Similar studies were performed to investigate the swelling behavior of end-grafted brush polymers. Polymer brushes are formed if the monomer density in an end-grafted polymer layer becomes sufficiently large causing the chains to stretch away from the surface. Because one end of the polymer chain is tethered to the substrate, Koga et al explored whether this confinement of the chain ends leads to a different conformation than that of the free-chain situation in $scCO_2$. The equilibrium brush structure is determined by a balance between the interactions that promote stretching of the polymer chains and the associated loss of chain conformational entropy. In addition, because polymer brushes can stretch without being removed from the substrate even in a good solvent, the solvent quality of density fluctuating $scCO_2$ could be investigated on the basis of the chain conformation perpendicular to the grafting surface. Using in-situ NR, a quantitative study of the solvent quality of $scCO_2$ was performed near the locus of maximum density inhomogeneity. The NR study showed that the solvent quality of density fluctuating $scCO_2$ for deuterated polystyrene (dPS) was still poor at the ridge condition where the excess swelling (~30%) occurred.

1.4. The Effect of Polymer Elasticity and Crystallinity on Swelling

From the theories of Flory and Huggins, polymer chain length and chain flexibility, significantly influence the entropy of mixing. The mixing of polymers with solvents is said to be more favorable as the chain size decrease because the entropy of mixing is greater. Flexible chains were also described as producing greater entropy of mixing, and stiff chains tended towards phase separation in mixtures. Similarly, comparisons of swelling behavior between glassy and rubbery amorphous polymer thin films have shown that the magnitude of anomalous swelling subsequent to $scCO_2$ exposure is also a function of initial elasticity. Accordingly, it is believed that to witness maximum density dilation, the polymer must exist in a rubbery state. In crystalline polymers, it was found that the extent of crystallization could affect anomalous behavior. Li et al. reports an unusually small degree of swelling in crystalline polyethylene oxide (PEO) analogous to the higher solubility of CO_2 in amorphous PEO reported by Weidner et al. The anomalous maxima, though evident, are significantly suppressed by the crystalline structure. The ability for $scCO_2$ to swell polymer thin films is a function of the fluid's ability to fully penetrate the film at the interface and diffuse throughout. For crystalline thin films, its rigid structure is believed to retard this behavior, thus swelling is less pronounced.

1.5. Research Approach and Organization

This report discusses novel methods for utilizing $scCO_2$ for the processing of polymer thin films and brushes. We investigated a number of polymer systems (amorphous homopolymer, semi-crystalline homopolymer, and brush polymer) supported on silicon substrates fabricated using different methods, including spin casting and chemical vapor

deposition. Thicknesses of films and brushes were typically below 1000 Å of various molecular weights.

Polymer systems were exposed to $scCO_2$ in a high-pressure cell. The body of the high-pressure cell was machined from 4340 steel. Sapphire was selected for the optical window material because of high transparency for neutrons. Furthermore, sapphire has high tensile strength (elastic limit 448 MPa), resistance to corrosion, high-energy damage threshold, and low absorbance. Two cylindrical sapphire windows (2.4 cm in thick, o.d. 5 cm) were installed for transmitting the incident beam and for receiving the reflected beams. The sealing was achieved by a combination of Teflon and a nylon gasket placed between the sapphire windows. The cell had a volume of about 10 mL and a maximum pressure rating of 140.0 MPa. CO_2 used in this study has a purity of 99.9%. CO_2 was loaded into the cell by means of a hand-operated syringe pump (HIP Equip.) to the desired pressure. Prior to pressurization, the air space is purged with the gas at low pressure. An OMEGADYNE pressure transducer (TH-1) with a pressure gauge meter (INFS-0001-DC1) was used to monitor the CO_2 pressure inside the cell. The temperature of the cell was controlled by a temperature controller (CAL Controls) equipped with heaters that were installed on the outer side of the cell and a thermocouple (Rama Co.). The temperature of the system was controlled with an accuracy of ±0.1 °C, and the stability of pressure during the measurements was less than ±0.2%.

The behaviors of the polymers were investigated using high-energy neutron and X-ray spectroscopic techniques. For the polymer brush systems, in situ neutron reflectivity was used to project the effects of density fluctuations on the solubility of $scCO_2$. The conformation and swelling of the polymer were also investigated to determine the role of CO_2-philicity in processing with $scCO_2$. From the reflectivity profiles, thickness, scattering length density, and

interfacial width/ roughness, of the polymer could be determined. Density profiles were modeled to project changes in polymer concentration as a function of the CO_2 solvent quality.

Various X-ray techniques were utilized to examine polymer thin films prior to and subsequent to $scCO_2$ exposure. The quick evaporation of CO_2 from the high-pressure cell to atmospheric pressure allows us to maintain the film's swollen structure. The films are stable at room temperature, which allows us to use techniques such as x-ray reflectivity and grazing incidence diffraction to probe the properties enhanced by $scCO_2$. X-ray reflectivity profiles provide insight into deviations of the film's thickness, density, and interfacial properties after exposure to $scCO_2$.

For our investigations on the enhancing the density dependent properties of polymer thin films, spectroscopic ellipsometry is employed. The ellipsometry measurements yielded changes in the film's thickness and the polymer's index of refraction (n_f). The difference witnessed in n_f can be used to correlate changes in the density dependent properties of the polymer.

Atomic force microscopy (AFM) is a powerful tool used to probe the topography of films. Three-dimensional topographical images of the films were produced to insure that no void or other dewetting structures were formed. From the images, cross-sectional analysis and surface roughness measurements were also performed to visually inspect the effects of $scCO_2$ on the film quality.

1.6. References:

[1] M. A. McHugh, and V. Krukonis, *Supercritical Fluids Extraction Principles and Practice* (Woburn, MA, 1994).

[2] G. Brunner, *An Introduction to Fundamentals of Supercritical Fluids and their Applications to Separation Processes* (SteinKopft Darmstadt, New York, 1994).

[3] *Supercritical Fluid Science: Fundamentals and Applications* (ACS Symp. Ser., 1993), Vol. 514.

[4] J. M. DeSimone, X. Guan, and C. S. Elsbernd, Science **257**, 945 (1992).

[5] T. Koga, Y. S. Seo, Y. Zhang, K. Shin, K. Kusano, K. Nishikawa, M. H. Rafailovich, J. C. Sokolov, B. Chu, D. Peiffer, R. Occhiogrosso, and S. K. Satija, Phys. Rev. Lett. **89**, 125506 (2002).

[6] T. Koga, Y. S. Seo, X. Hu, S. Kwanwoo, Y. Zhang, M. H. Rafailovich, J. C. Sokolov, B. Chu, and S. K. Satija, Europhys. Lett. **60**, 559 (2002).

[7] T. Koga, Y. S. Seo, K. Shin, Y. Zhang, M. Rafailovich, J. Sokolov, B. Chu, D. Peiffer, and S. K. Satija, Macromolecules **36**, 5236 (2003).

[8] T. Koga, Y. Ji, Y. S. Seo, M. H. Rafailovich, J. C. Sokolov, and S. K. Satija, J. Polym. Sci, Part B:Polym. Phys. **42**, 3282 (2004).

[9] T. Koga, Y. S. Seo, J. Jerome, S. Ge, M. H. Rafailovich, J. C. Sokolov, B. Chu, O. H. Seeck, M. Tolan, and R. Kolb, Appl. Phys. Lett. **83**, 4309 (2003).

[10] T. Koga, J. Naisheng, P. Gin, M. Endoh, S. Narayanan, L. Lurio, and S. K. Sinha, Phys. Rev. Lett. **107**, 225901 (2011).

[11] T. Koga, C. Li, M. K. Endoh, J. Koo, M. H. Rafailovich, S. Narayanan, D. R. Lee, L. Lurio, and S. K. Sinha, Phys. Rev. Lett. **104**, 066101 (2010).

[12] Y. Fujii, Z. Yang, J. Leach, H. Atarashi, K. Tanaka, and O. Tsui, Macromolecules **42**, 7418 (2009).

[13] S. C. Tucker, Chem. Rev. **99**, 391 (1999).

[14] H. E. Stanley, *Introduction to Phase Transition and Critical Phenomena* (Oxford University Press, Oxford, 1971).

[15] C. A. Eckert, D. H. Ziger, K. P. Johnston, and S. Kim, J. Phys. Chem. **90**, 2738 (1986).

[16] J. A. Gates, R. H. Wood, and J. R. Quint, J. Phys. Chem. **86**, 4948 (1982).

[17] C. A. Eckert, D. H. Ziger, K. P. Johnston, and T. K. Ellison, Fluid Phase Equilib. **14**, 167 (1983).

[18] D. B. McGuigan, and P. A. Monson, Fluid Phase Equilib. **57**, 227 (1990).

[19] E. H. Chimowitz, and G. Afrane, Fluid Phase Equilib. **120**, 167 (1996).

[20] K. S. Shing, and S. T. Chung, AIChE **34**, 1973 (1989).

[21] A. A. Chialvo, and P. T. Cummings, AIChE **40**, 1558 (1994).

[22] K. Nishikawa, I. Tanaka, and Y. Amemiya, J. Phys. Chem. **100**, 418 (1996).

[23] T. Morita, K. Kusano, H. Ochiai, K. Saitow, and K. Nishikawa, J. Chem. Phys. **112**, 4203 (2000).

[24] K. Nishikawa, and T. Morita, Chem. Phys. Lett. **316**, 238 (2000).

[25] M. Kamiya, K. Muroki, and M. Uematsu, J. Chem. Thermodyn. **27**, 337 (1995).

[26] Z. Chen, K. Tozaki, and K. Nishikawa, Jpn. J. Appl. Phys. **38**, 6840 (1999).

[27] E. F. Carome, C. B. Cykowski, J. F. havlice, and D. A. Swyt, Physica **38**, 307 (1968).

[28] C. A. Eckert, B. L. Kuntson, and P. G. Debenedetti, Nature **383**, 313 (1996).

[29] T. P. Russell, Mater. Sci. Rep. **5**, 171 (1990).

[30] G. K. Fleming, and W. J. Koros, Macromolecules **19**, 2285 (1986).

[31] R. G. Wissinger, and M. E. Paulaitis, J. Poly. Sci. Polym. Phys. Ed. **25**, 2497 (1987).

[32] J. J. Shim, and K. P. Johnston, AIChE J. **35**, 1097 (1989).

[33] B. J. Briscoe, and S. Zakaria, J. Polym. Sci. : Part B. **29**, 989 (1991).

[34] S. K. Goel, and E. J. Beckman, Polymer **34**, 1410 (1993).

[35] A. Garg, E. Gulari, and W. Manke, Macromolecules **27**, 5643 (1994).

[36] Y. Zhang, K. K. Gangwani, and R. M. Lemert, J. Supercritical Fluids **11**, 115 (1997).

[37] S. H. Chang, S. C. Park, and J. J. Shim, J. Supercritical Fluids **13**, 113 (1998).

[38] J. R. Royer, J. M. DeSimone, and S. A. Khan, Macromolecules **32**, 8965 (1999).

[39] T. Koga, J. L. Jerome, Y.-S. Seo, M. H. Rafailovich, J. C. Sokolov, and S. K. Satija, Langumuir **21**, 6157 (2005).

[40] K. A. Arora, A. J. Lesser, and T. J. McCarthy, Macromolecules **31**, 4614 (1998).

[41] C. M. Stafford, T. P. Russell, and T. J. McCarthy, Macromolecules **32**, 7610 (1999).

[42] T. Koga, E. Akashige, M. H. Rafailovich, J. C. Sokolov, K. Shin, Y. Seo, S. K. Satija, and B. Chu, Physica B **357**, 73 (2005).

[43] T. Koga, J. L. Jerome, C. Gordon, M. H. Rafailovich, and J. C. Sokolov, Journal of Adhesion **81**, 751 (2005).

[44] S. M. Sirard, Z. K. J., I. C. Sanchez, P. F. Green, and K. P. Johnston, Macromolecules **35**, 1928 (2002).

[45] Y. Li, E. Park, K. T. Lim, K. P. Johnston, and P. F. Green, J. Polym. Sci, Part B:Polym. Phys. **45**, 1313 (2007).

[46] X. Wang, and I. C. Sanchez, Langumuir **22**, 9251 (2006).

CHAPTER II

Generality of Anomalous Expansion of Polymer Chains in Supercritical Fluids

Polymer Volume 52, Issue 19, 1 2011, Pages 4331-4336

Abstract:

By using in-situ neutron reflectivity, we have investigated swelling isotherms of solvophilic and solvophobic end-grafted/non-grafted polymer chains on solid substrates in supercritical carbon dioxide and supercritical ethane. It was found that anomalous expansion of the polymer chains associated with excess absorption of the fluid molecules occurs in the large compressible regions of both supercritical fluids (SCFs) regardless of the polymer-fluid interactions. Furthermore, when the solvent quality of the SCFs with the polymer is nearly identical, the anomalous expansion of the polymer chains can be scaled with the magnitude of long-range density fluctuations in the pure SCF phases. A simple thermodynamic two-state model along with the experimental results proposes that polymer chains are expanded independently of the polymer-fluid interactions to further change solvent-density fluctuations around the polymer chains, thereby lowering the free energy of the polymer/SCF systems.

2.1 Introduction

What makes supercritical fluids (SCFs) novel solvents is the formation of a local solvent density inhomogeneity around a solute. Thus the local solvent density is enhanced from the average bulk density when the solvent-solute interaction is favorable and depleted in cases of unfavorable interactions[1]. Kim and Johnston have first demonstrated that the local solvent density is highest in the region of the highest compressibility near the critical points of various SCFs[2]. Near the critical point, microscopic thermal fluctuations of molecules become strongly correlated, leading to large-scale, coherent density fluctuations[3]. Since the isothermal compressibility (κ_T) is directly related to long-range density fluctuations in SCFs, the highest compressibility region corresponds to the region with the largest density fluctuations, known as "density fluctuation ridge" in a SCF state[4]. The ridge emanates from the critical point where the amplitude of the density fluctuations diverge, and separates the more liquid-like and more gas-like regions in the supercritical region[4,5]. In the region below the critical point, the ridge corresponds to the vapor line. In the supercritical region, there is a memory of the vapor line, i.e. the ridge. This ridge is not only specific to CO_2. It is a general feature for substances, such as H_2O, CF_3H, Ar and Hg [5]. It is also known that the ridge corresponds to a maximum or minimum of thermal conductivity[6], sound velocity[7], and partial molar volumes[8,9]. In addition, the rate constants or equilibrium constants of various chemical reactions in SCFs show maxima, minima or inflection points at the ridge[9].

So far, only few theoretical[10] and numerical simulation[11] results have been reported on a thermodynamically stable conformation of a single polymer chain in such solvation structures. Dua and Cherayil[10] showed that on approaching the liquid-vapor critical point, a polymer chain first collapses and then subsequently returns to its original dimensions, which is qualitatively

consistent with the Brochard and de Gennes's prediction for a polymer chain in a binary solvent mixture near the critical point[12]. On the other hand, multiscale simulation[13] predicted excess expansion of a single polymer chain in a SCF regardless of solute-solvent interactions when the solvent's compressibility becomes larger. Sumi et al. proposed that an increase in the local solvent density around a solvophilic polymer chain or the formation of a large correlation hole around a solvophobic polymer chain (i.e., excluding the fluid molecules around the polymer chain) is induced and the polymer chain in the solvation structures is anomalously expanded as a thermodynamically stable state[13]. This expansion causes additional large solvent-density fluctuations around the polymer chain over a large area compared with the correlation length of the solvent molecules, thus lowering the free energy of a SCF/polymer system[1].

On the other hand, by using a in-situ neutron reflectivity (NR) technique, we have previously revealed that concentrated deuterated polystyrene (d-PS) chains grafted on Si substrates (i.e., polymer brushes) show anomalous expansion of the chains in the vicinity of the density fluctuation ridge of supercritical carbon dioxide ($scCO_2$, the critical point is $T_c = 31.3°C$ and $P_c = 7.38$ MPa)[14]. In addition, the volume fraction profiles of the d-PS brushes within the entire pressure range (0.1MPa < P < 20MPa) could be approximated by a simple step function, indicating that the solvent quality of $scCO_2$ for d-PS is still poor even at the ridge condition. Moreover, the pressure dependence of the brush heights including near the density fluctuation ridge condition is exactly identical to the linear dilation (in the direction normal to the surface) isotherm of spun cast (non-grafted) d-PS thin films in $scCO_2$[15,16]. Consequently, it is reasonable to say that the anomalous swelling of various spun cast polymer thin films reported[15-17] is attributed to the excess expansion of polymer chains themselves rather than the presence of an

adsorption layer of CO_2 molecules on the film surface (a few nanometer in thick) predicted by Wang and Sanchez[18].

Motivated by the previous theoretical work[13], the present study aims to establish generality of the excess expansion of polymer chains in SCFs. Here we show that the anomalous expansion occurs near the density fluctuation ridges of $scCO_2$ and supercritical ethane (scC_2H_6, T_c =32.4 °C, P_c = 4.9 MPa) regardless of their miscibility with polymers. In addition, we found that the excess expansion of solvophobic polymer chains in both SCFs collapse onto one master curve under the same magnitude of density fluctuations in the fluids. Moreover, the magnitude of density fluctuations, where the excess expansion of the polymer chains takes place, is in good agreement with that predicted for a single polymer chain[13]. Therefore it is anticipated that the origin of the anomalous expansion of the concentrated polymer chains in the present study is also the formation of the unique solvation structures depending on the polymer-fluid interactions. In order to further understand the mechanism of the anomalous expansion of the polymer chains, we introduce a simple two-state model which is phenomenologically similar to the one for protein folding to determine the conformational stability of a molecule originally proposed by Anson[19]. This two-state model, which assumes that polymer chains belong to only two thermodynamic states (an excess swollen state and non-excess swollen state), along with the experimental data suggests that the strength of the excess absorption of the fluid molecules into a polymer matrix is altered (stronger or weaker) across the density fluctuation ridge independently of the polymer-fluid interactions. Furthermore, the model points to a significant volume change of the entire system between the two states at the ridge condition, suggesting the emergence of a large change in the compressibility. Hence, this supports the aforementioned mechanism that the

large change in the compressibility induced by the excess expansion of polymer chains is crucial for stabilizing the free energy of the entire system.

2.2 Experimental Section

2.2.1 Materials. In order to provide a better understanding of the anomalous expansion of polymer chains, the following two polymer systems were chosen: (i) a solvophilic (or "CO_2-philic") polymer brush, in which one end of polymer chains is chemically grafted to a solid substrate, such that we can directly discuss chain conformations even in a good solvent; (ii) non-grafted solvophobic polymer chains in the two different SCFs with nearly identical solvent qualities with the polymer. Note that the anomalous expansion of end-grafted and non-grafted polymer films has been proven to be identical[14]. For the system (i), an amorphous poly{2-(perfluorobutyl)ethyl acrylate} (PFA-C_4, M_w=304,000, M_w/M_n=1.3) brush was prepared by surface-initiated atom transfer radical polymerization (ATRP)[20] on a Si substrate (8-mm thickness and 75-mm diameter) for the NR study. The PFA-C_4 polymer brush, for which the perfluoroalkyl chains have good miscibility with CO_2, has a high enough neutron scattering length density (SLD) contrast such that deuterium labeling was not necessary. The thickness of the unswollen PFA-C_4 film, which was dried in a vacuum oven for 2 h at 120 °C in order to remove the solvent used for the polymerization, was determined to be 585 Å by using a spectroscopic ellipsometer (Nippon Laser & Electronics Lab.) (assuming index of refraction =1.36) and further confirmed by NR experiments. This thickness corresponds to a grafting density of 2.1×10^{-3} chains/Å^2. For the system (ii), deuterated polybutadiene (d-PB, M_w=240,000, M_w/M_n=1.05, Polymer Source Inc.) films were spun cast from toluene solutions onto HF etched

Si substrates and then dried in a vacuum oven for 4 h at 120 °C to relax strains induced in the spinning process. The original thickness of the d-PB films was about 350 Å determined by a spectroscopic ellipsometer (Rudolph Electronics, AutoEL-II) equipped with a He-Ne laser (632 nm) (assuming index of refraction =1.42) and NR. The d-PB films were exposed to $scCO_2$ and scC_2H_6 (both of which are poor solvents within the pressure range used in this study) and its swelling behavior was characterized by NR as a function of temperature and pressure. Note that ethane dissolves PB when the pressure is high enough (~100 MPa), while CO_2 does not dissolve PB regardless of pressure (up to 300 MPa) and temperatures (up to 200°C)[21]. However, as discussed below, ethane is a poor solvent for PB within the pressure range used in this study.

2.2.2 Neutron Reflectivity (NR) Measurements.

Specular reflectivity measurements were performed on the NG7 neutron reflection spectrometer at the National Institute of Standards and Technology (NIST) with a wavelength (λ) of 4.76 Å and a $\Delta\lambda/\lambda$ of 2.5 %. A high pressure cell used for NR measurements was designed and built by the High Pressure Equipment Co. (PA, USA)[16]. The NR experiments with the high pressure cell were conducted under the respective isothermal conditions (T = 36 °C for CO_2 and T = 37.2 °C for C_2H_6) with elevated pressures up to P = 21 MPa in order to compare the swelling behaviors under the same magnitude of density fluctuations in both SCFs, as described below. The films were exposed to CO_2 or C_2H_6 for up to 4 h prior to data acquisition in order to ensure that equilibrium swelling was achieved. Data was obtained both by successively increasing the pressure and then slowly decreasing the pressure. The results were identical, indicating that all the swelling isotherms were reversible with pressure and temperature. Since the background scattering from pure CO_2 and C_2H_6 phases increased dramatically near the critical points, we

measured the scattering from the pure fluid phases (i.e., the long-range density fluctuations) for each pressure condition. The NR data corrected for the background scattering was analyzed by comparing the observed reflectivities with the calculated ones based on model scattering length density (SLD) profiles. The SLD profiles were subsequently converted to the corresponding polymer volume fraction profiles. Assuming that the concentration of the mixture is homogenous through the entire film, the SLD value of the polymer/SCF system is defined by

$$SLD_{mix}(z) = SLD_{polymer} \times \phi(z) + SLD_{SCF} \times (1 - \phi(z)) \qquad (2\text{-}1)$$

where SLD_{mix} is the *SLD* value of the mixture at a distance z from the substrate, SLD_{polymer}, and SLD_{SCF} are the pure component *SLD*'s of the polymer thin films and CO_2, respectively, and *f(z)* is the volume fraction of the polymer at a distance z from the substrate. The density of CO_2 dissolved in the polymers was taken to be 0.956 g/cm^3 since the molar volume of CO_2 within the polymer can be much different from the molar volume of the bulk CO_2[22]. To ensure conservation of mass, the volume fraction profiles were calculated such that the same amount of the polymer chains remains at all solvent concentrations.

2.3 Results and Discussion

Fig. 2-1 (a) shows representative NR profiles for the PFA-C_4 polymer brush at the four different pressures at T = 36 °C; the reflected intensity is plotted as a function of the momentum transfer normal to the surface, $q_z = 4 \pi \sin\theta / \lambda$, where q is the glancing angle of incidence and l is the neutron wavelength (4.7 Å). The solid lines correspond to the best-fits to the data based on the volume fraction profiles of the polymer chains, *f(z),* shown in Fig. 2-1 (b). The profiles of the PFA-C_4 brush film were generated from the self-consistent field calculation[23]:

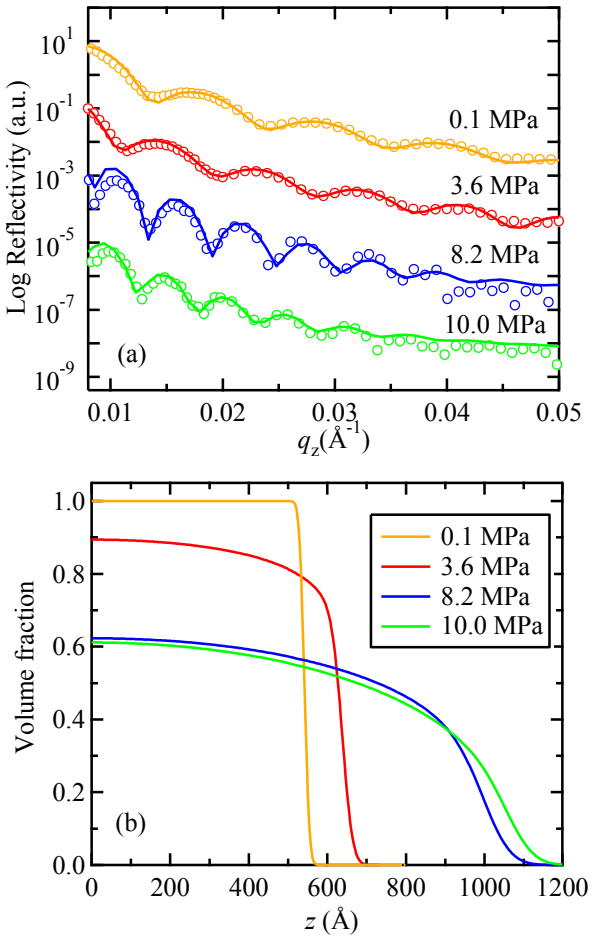

Figure 2-1. (a) Representative NR curves (circles) for the PFA-C_4 brush at different CO_2 pressures. Consecutive reflectivities have been offset from each other for clarity. The solid lines correspond to the calculated reflectivities based on the volume fraction profiles of the PFA-C_4 brush shown in (b).

$$\phi(z) = \begin{cases} \phi_s[1-(z/h)^2]^{\alpha}, z < h \\ 0, z > h \end{cases} \quad (2\text{-}2)$$

where f_s is the polymer volume fraction at the silicon oxide surface, h is the cutoff thickness of the profile, and α is the "profile exponent", which is a measure of the solvent quality. In addition, a tail was introduced to fit the data by convoluting eq. (2-2) with a normalized Gaussian function having a full width at half maximum Δ (tail width) in a region spanning nearly ± 2Δ about the cutoff length[24]. In the limit of infinitely long chains[23], the values, α = 1 (a parabolic shape) for a good solvent, α = 0.5 for a θ solvent, and α = 0 (a step function) for an extremely poor/non-solvent, are predicted. As shown in Fig. 2-1(a), good fits to the data were obtained with uniform concentrations in the polymer layer without any preferential adsorption of either CO_2 or polymer at the Si substrate. The thickness of the layer, which was initially 585Å, increased to 1117 Å at P = 8.2 MPa and then further increased to 1420 Å upon compression to P = 20.8 MPa.

Figure 2-2 (a) shows the linear expansion of the brush calculated by the equation, $l_h = (h_1 - h_0)/h_0$, where h_1 and h_0 are the measured heights of the swollen and unswollen polymer brush, respectively. From the figure we can see that the l_h values increase up to 1.4 and the volume fraction profiles change to nearly parabolic shapes at high pressures (i.e., $a \sim 1$) as shown in Fig 2-2 (b), indicating that the solvent quality of $scCO_2$ for the PFA-C_4 brush is improved significantly as pressure increases. This is further confirmed by the variation of the tail width (Δ) as a function of pressure (Fig. 2-2(c)). The interfacial width between the polymer and CO_2 layers, which was initially 50 Å at atmospheric pressure, increased to almost 200 Å at P = 20.8 MPa. At the same time, a noticeable anomalous peak is present in l_h near the density fluctuation ridge (P_{ridge} = 8.2 MPa at T =36 °C for CO_2)[4] where excess swelling of not only "CO_2-phobic" spin-

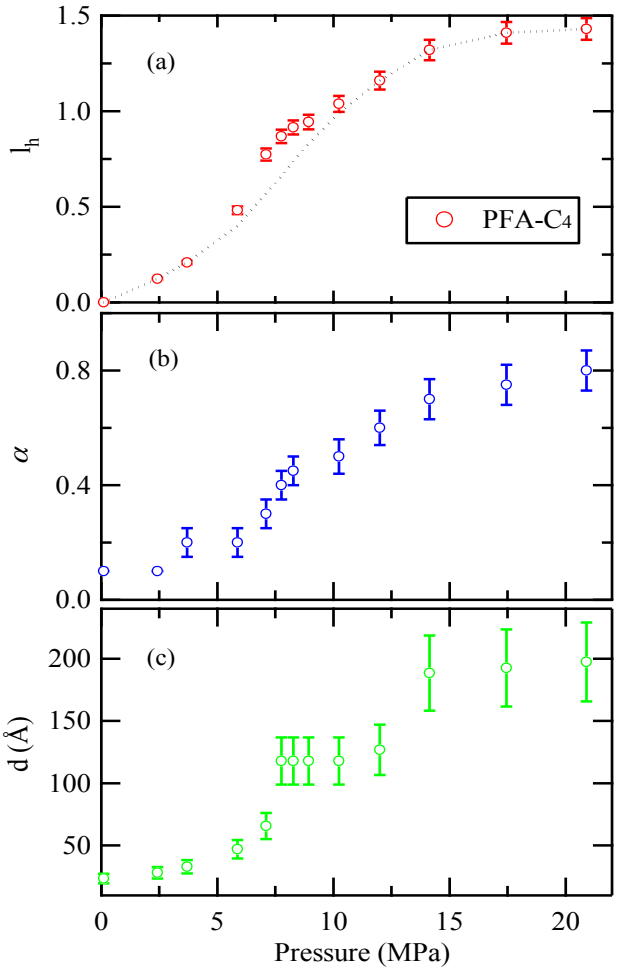

Figure 2-2. Pressure dependences of (a) the measured height (l_h), (b) the profile exponent (a), and (c) the tail width (**Δ**) of the swollen PFA-C_4 brush in CO_2 obtained by the best-fits of the calculated reflectivities based on eq. (2-2) in the text to the observed reflectivities. The error bars are obtained from the fitting procedure. The dotted line in Fig. 2(a) corresponds to non-excess swelling estimated by interpolating the data on either side of the anomalous maximum.

cast (non-grafted) polymer thin films[15-17] but also a CO_2-phobic deuterated polystyrene (d-PS) brush[14] has occurred. Hence, the present NR results clarify that polymer chains are anomalously expanded in $scCO_2$ irrespective of their miscibility with $scCO_2$, as predicted for a single polymer chain in a SCF medium[13]. In addition, we found the a value at the ridge is close to 0.5, indicating that $scCO_2$ becomes a θ-solvent for the PFA-C_4 brush. It should be added that the width of the brush tail at the ridge (Δ=120Å) is in good agreement with that for the PS brush at the θ temperature in deuterated cyclohexane (Δ~130Å)[24].

Next, we aim to further extend the generality of the anomalous expansion of polymer chains by comparing the two SCFs. To extract the role of the long-range density fluctuations in the anomalous expansion, we used spun cast d-PB polymer films, which have poor miscibility with both SCFs, and mimicked the magnitude of the density fluctuations in both SCFs by using the scaled T and P conditions[25]. As shown in Fig. 2-3, this mimic was confirmed by our calculations using the following equation:

$$\left\langle \Delta N^2 \right\rangle / \left\langle N \right\rangle = (N/V)\kappa_T k_B T \qquad (2\text{-}3)$$

where N is the number of molecules in the corresponding volume V, κ_T is the isothermal compressibility, and k_B is the Boltzmann constant. For this study, the κ_T values were calculated using the modified Benedict-Webb-Rubin equation of state for ethane[26] and the empirical equation of state derived by Huang et al. for CO_2[27]. We also confirmed that the linear dilation of the spun cast d-PB films was exactly identical to the linear expansion of end-grafted d-PB brushes in both SCFs, as reported for the d-PS thin films described above. The details of the swelling behavior of the d-PB brushes will be described elsewhere.

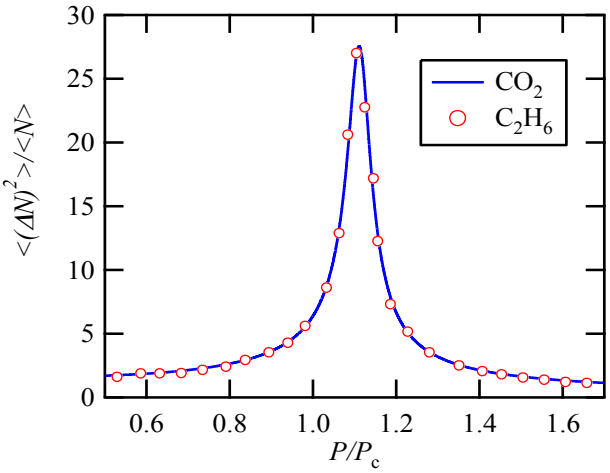

Figure 2-3. Calculated density fluctuations in CO_2 and C_2H_6 vs. scaled pressure by P_c at T=1.15T_c.

Fig. 2-4 (a) shows the pressure dependence of the swelling isotherms for the spin cast d-PB thin films at T = 36 °C for CO_2 and T = 37.2 °C for C_2H_6 (both conditions correspond to T/T_c = 1.15) measured by NR. The experimental data for the d-PB thin films were analyzed by comparing the observed reflectivities with calculated ones based on a hyperbolic-tangent model density profile[28], since, as shown in the inset of Fig. 2-4(a), the volume fraction profiles of the d-PB thin films in both CO_2 and C_2H_6 could be approximated as a step function (i.e., a = 0 in eq. (2-2)) at all the experimental conditions. This indicates that the solvent qualities of both SCFs for d-PB are poor even at the density fluctuation ridge based on the interfacial structures. The linear dilation (in the direction normal to the surface) of spin cast d-PB films was calculated by the equation, $l_f = (L_1-L_0)/L_0$, where L_1 and L_0 are the measured thickness of the swollen and unswollen polymer thin films, respectively. From the figure we can see that the magnitude of the anomalous swelling maximum at the ridge of C_2H_6 (P_{ridge} = 5.4 MPa) was much higher (l_f = 1.2) than that at the ridge of CO_2 (l_f = 0.8). However, this is attributed to the difference in the "inherent" swelling (related to the bulk miscibility) of the d-PB films (indicated by the dotted lines) in both SCFs, as shown in Fig. 2-4 (a). The dotted lines in the figure correspond to the "non-excess (bulk)" swelling in both CO_2 and C_2H_6 (l_b) simulated by pressing a 1-mm thick disk of brominated poly{isobutylene-*co*-(*p*-methylstyrene)} (BIMS) directly onto the d-PB thin film[15]. Since the anomalous dilation is a surface effect which occurs only within ~10 R_g (R_g is the radius of polymer gyration) of the polymer/CO_2 interface[15], the BIMS layer, which was not deuterated for the NR experiments, served as a "cap" for the bottom d-PB film to eliminate the anomalous dilation. The excess swelling (l_e) values, which were obtained by subtracting l_b from

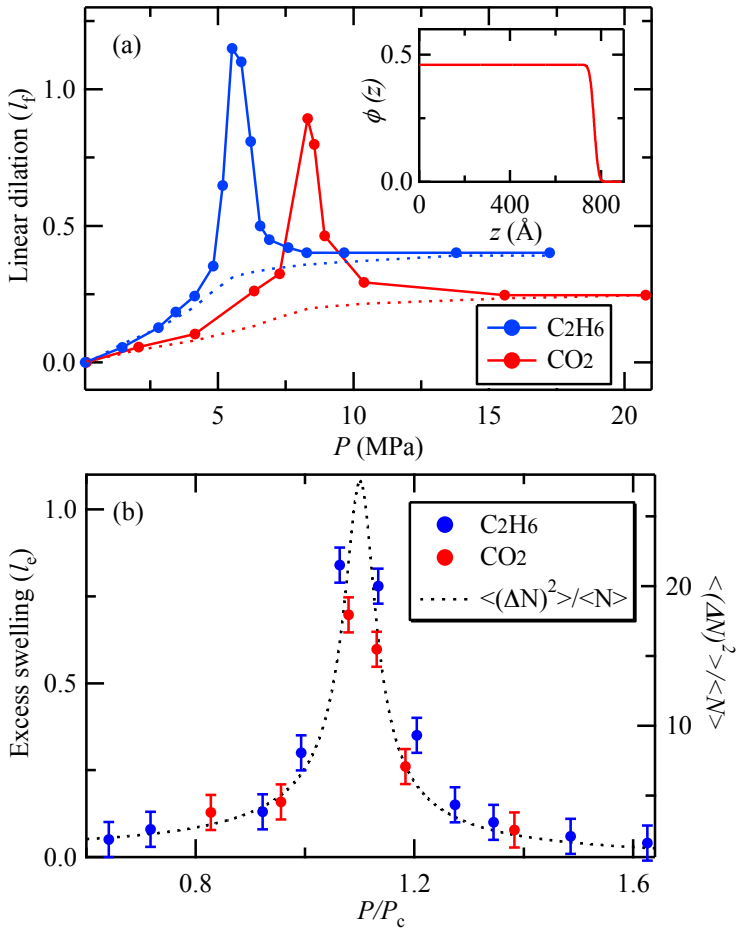

Figure 2-4. (a) Pressure dependence of the swelling isotherms for the d-PB thin films in CO_2 and C_2H_6 at T=1.15T_c. The dotted lines correspond to "bulk" swelling of the d-PB thin films in both SCFs. In the inset, the volume fraction profile at the ridge condition of C_2H_6 is shown. (b) Excess swelling of the d-PB thin films in CO_2 and C_2H_6 are shown along with density fluctuations in both SCFs.

the linear dilation data (l_f), are plotted in Fig. 2-4 (b). We can see that the magnitudes of the excess swelling of the d-PB thin films in both SCFs are almost identical each other and follow

the locus of the density fluctuations in both SCFs when superimposed by the scaled temperature and pressure. Consequently, the NR results elucidate that the excess expansion of the solvophobic polymer chains occurs regardless of SCF choices and can be scaled with the magnitude of the density fluctuations in both SCFs. In addition, we found that the excess swelling appears in the compressed region of $0.7 \leq P/P_c \leq 1.65$ in both SCFs, which corresponds to $\langle \Delta N^2 \rangle / \langle N \rangle \geq 1.5$ ($\langle \Delta N^2 \rangle / \langle N \rangle = 1.0$ for an ideal gas). According to a previous report[4], $\langle \Delta N^2 \rangle / \langle N \rangle$ of 1.5 is equivalent to a correlation length of 5 Å for pure SCF molecules. Interestingly, this correlation length is in good agreement with theoretical work in which an anomalous expansion of a single solvophobic polymer chain occurs due to the local solvent density inhomogeneity in a SCF[13]. Hence, this consistency may lead to the conclusion that the origin of the anomalous expansion for the present experimental results and the previous simulation results on a single polymer chain is identical: it is attributed to the increase in the local solvent density around solvophilic polymer chains or the formation of a large correlation hole around solvophobic polymer chains. Within such solvation structures, polymer chains are expanded as a thermodynamically stable state so that additional large changes in solvent-density fluctuations around the polymer chains are induced, thus lowering the free energy of the entire SCF/polymer system[13].

In order to further understand the mechanism of the anomalous expansion driven by long-range density fluctuations in SCFs, we propose a simple thermodynamic model, which assumes that polymer chains belong to only two thermodynamic states, i.e., the excess swollen state

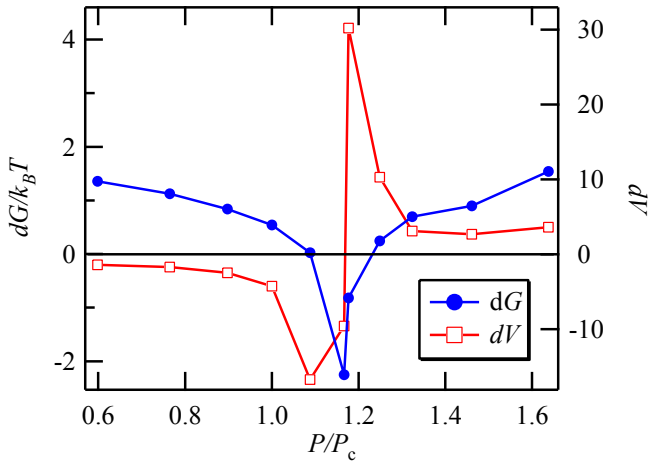

Figure 2-5. Pressure dependences of (blue circles) and (red squares) for the d-PB thin films in SCFs at T =1.15T_c. The values shown in Fig. 2-4 are used for determination of the equilibrium constant as described in the text.

(denoted by *E*) and non-excess swollen state (denoted by *N*). Similar two-state model has been widely used to determine the conformation stability of a protein molecule during the process of unfolding by gradually changing its environmental conditions[19]. Polymer chains may undergo the transition between the *E* and *N* states according to a simple kinetic model,

$$\mathrm{N} \rightleftharpoons \mathrm{E} \tag{2-4}$$

with rate constants k_N and k_E for the collapse of polymer chains and for the expanding of polymer chains, respectively. The difference in the Gibbs free energy between the *E* and *N* states is defined as $\Delta G = G_E - G_N$ and the total differentiation is then given by

$$d(\Delta G) = dP\Delta V - dT\Delta S\,, \tag{2-5}$$

where $\Delta V = V_E - V_N$ and $\Delta S = S_E - S_N$ are the changes in the volume and entropy of the entire system due to the anomalous expansion, respectively. ΔG is related to the equilibrium constant, $K_{ea} \equiv k_E / k_N = X_E / X_N$ via $\Delta G = -k_B T \ln K_{ea}$, where X_E and $X_N = 1 - X_E$ are probabilities of the *E* and *N* state, respectively. Since the NR technique is not suitable for time-resolved experiments to measure the kinetic rates under the *T* and *P* conditions of interest, we estimated the probabilities based on the experimental swelling data. To convert the swelling data into the probabilities, the following assumptions were made: the observed excess expansion can be decomposed into a weighted average composed of the two states,

$$l_e = X_E l_e^{\max} + (1 - X_E) l_e^{\min}\,, \tag{2-6}$$

where $l_e^{\max}$ and $l_e^{\min}$ correspond to the l_e value for the *E* and *N* state, respectively. The other assumption is that only the *E* state contributes to the excess expansion (i.e., $l_e^{\min} = 0$) and at the density fluctuation ridge all chains belong to the *E* state (i.e., X_{E} =1) such that $l_e^{\max}$ corresponds to the l_e value. With these assumptions, ΔG can be then simplified as follows:

$$\Delta G = -k_B T \ln\left[l_e / (l_e^{max} - l_e) \right]. \qquad (2\text{-}7)$$

Fig. 2-5 shows the pressure dependence of ΔG and $\Delta V = \left(\partial \Delta G / \partial P\right)_T$ calculated by the experimental l_e values shown in Fig. 2-4. As expected, ΔG becomes negative (and minimum) at around the ridge. The more important point is that ΔV is negative at the lower-pressure side of P_{ridge} (=1.15 P_c) during the pressurization process, while ΔV changes sign to positive after passing P_{ridge}. In other words, the amounts of the excess absorption of SCF molecules increases with increasing pressure at $P < P_{\mathrm{ridge}}$ and, in contrast, decreases with increasing pressure at $P > P_{\mathrm{ridge}}$. Hence, this two-state model proposes that the density fluctuation ridge is a unique environmental condition on the solvation property of SCFs for polymer chains: the strength of the excess absorption of the fluid molecules becomes stronger or weaker across the density fluctuation ridge independently of polymer-fluid interactions, resulting in the maximum chain expansion at the density fluctuation ridge. Furthermore, the significant change in ΔV at around the ridge is indicative of a large difference in compressibility between the *E* and *N* states. This supports the aforementioned mechanism that a high response of density fluctuations in SCFs to the conformation changes of flexible polymer chains is essential to lower the free energy of the entire system.

It should be pointed out that while the shapes and loci follow those of the density fluctuations, there are significant differences in the excess swelling maximum at the ridge among d-PB ("CO_2-phobic", $l_e = 0.55$), PFA-C_4 ("CO_2-philic", $l_e = 0.22$) and d-PS ("CO_2-phobic", $l_e \sim 0.1$[16]). This is inconsistent with the theoretical work for a dilute polymer solution[13]: The degree of anomalous expansion is larger as the polymer-solvent interaction becomes stronger. Rather, our results suggest that the elasticity or hardness of polymer films plays a crucial role in the magnitude of the excess swelling maximum for concentrated polymer chains in a density fluctuating SCF. Further experiments are currently in progress to clarify this point.

2.4 Conclusions

We have revealed the generality of excess expansion of concentrated polymer chains driven by large density fluctuations in supercritical fluids. It was found that the excess expansion occurs regardless of the miscibility of supercritical fluids with the polymers and the magnitude of the excess expansion collapse onto one master curve when the magnitude of density fluctuations of the fluids for the solvophobic polymer is fixed. In addition, we have clarified that the excess expansion appears in the compressed region of $0.7 \leq P/P_c \leq 1.65$ in both supercritical CO_2 and C_2H_6. This region has the magnitude of density fluctuations of more than 1.5 ($\left\langle \Delta N^2 \right\rangle / \left\langle N \right\rangle \geq 1.5$), which is equivalent to a correlation length of more than 5Å for pure SCF molecules[4]. The size of the correlation length is in good agreement with that predicted for anomalous expansion of a single polymer chain in a SCF[13]. This consistency may draw the conclusion that the origin of the anomalous expansion of the concentrated polymer chains is additional large solvent-density fluctuations induced by the conformation changes too, thereby

lowering the free energy of the entire SCF/polymer system. In order to further understand the mechanism, we propose a simple thermodynamic model which assumes that polymer chains belong to only two thermodynamic states (the excess swollen state and non-excess swollen state). Although the quantitative propriety of the two-state model or the statistical mechanics expression of the probabilities for both states is not quite conclusive yet, the model points to a large difference in the volume change of the entire system at the ridge condition, indicating the occurrence of large changes in the compressibility. Hence this supports the previous theoretical work that the large change in the compressibility induced by the expanded conformation of flexible polymer chains is key for the thermodynamic stability in the presence of large solvent density fluctuations.

2.5 References

[1] S.C. Tucker, Chem. Rev. **99**, 391 (1999).

[2] S. Kim and K. P. Johnston, Ind. Eng. Chem. Res. **26**, 1206 (1987).

[3] H. E. Stanley, *Introduction to Phase Transition and Critical Phenomena*. (Oxford University Press, Oxford, 1971).

[4] K. Nishikawa, I. Tanaka, and Y. Amemiya, J. Phys. Chem. **100**, 418 (1996).

[5] K. Nishikawa and T. Morita, Chem. Phys. Lett. **316**, 238 (2000).

[6] Z. Chen, K. Tozaki, and K. Nishikawa, Jpn. J. Appl. Phys. **38**, 6840 (1999).

[7] E. F. Carome, C.B. Cykowski, J.F. havlice, and D.A. Swyt, Physica **38**, 307 (1968).

[8] C. A. Eckert, D. H. Ziger, K. P. Johnston, and S. Kim, J. Phys. Chem. **90**, 2738 (1986).

[9] C. A. Eckert, B. L. Kuntson, and P. G. Debenedetti, Nature **383**, 313 (1996).

[10] A. Dua and B.J. Cherayil, J. Chem. Phys. **111**, 3274 (1999).

[11] G. Luna-Barcenas, J.C. Meredith, I.C. Sanchez, K.P. Johnston, D.G. Gromov, and J.J. de Pablo, J. Chem. Phys. **107**, 10782 (1997); G. Luna-Barcenas, D.G. Gromov, J.C. Meredith, I.C. Sanchez, J.J. de Pablo, and K.P. Johnston, Chem. Phys. Lett. **278**, 302 (1997).

[12] F. Brochard and P.G. de Gennes, Ferroelectrics **30**, 33 (1980).

[13] T. Sumi and H. Sekino, J. Chem. Phys. **122**, 194910 (2005); T. Sumi, N. Imazaki, and H. Sekino, Phys. Rev. E **79**, 030801 (2009).

[14] T. Koga, Y. Ji, Y.S. Seo, M.H. Rafailovich, J.C. Sokolov, and S. K. Satija, J. Polym. Sci, Part B:Polym. Phys. **42**, 3282 (2004).

[15] T. Koga, Y.S. Seo, Y. Zhang, K. Shin, K. Kusano, K. Nishikawa, M.H. Rafailovich, J.C. Sokolov, B. Chu, D. Peiffer, R. Occhiogrosso, and S. K. Satija, Phys. Rev. Lett. **89**, 125506 (2002).

[16] T. Koga, Y.S. Seo, K. Shin, Y. Zhang, M. Rafailovich, J. Sokolov, B. Chu, D. Peiffer, and S. K. Satija, Macromolecules **36**, 5236 (2003).

[17] S. M. Sirard, Ziegler K. J., I. C. Sanchez, P. F. Green, and K.P. Johnston, Macromolecules **35**, 1928 (2002); Y. Li, E. Park, K. Lim, K.P. Johnston, and P. F. Green, J. Polym. Sci. Part B. Polym. Phys. **45**, 1313 (2007).

[18] X. Wang and I.C. Sanchez, Langmuir **22**, 9251 (2006).

[19] M.L. Anson, Adv. Protein Chem. **2**, 361 (1945).

[20] H. Yamaguchi, K. Honda, M. Kobayashi, M. Morita, H. Masunaga, O. Sakata, S. Sasaki, and A. Takahara, Polymer J. **40**, 854 (2008).

[21] C. F. Kirby and M. A. McHugh, Chem. Rev. **99**, 565 (1999).

[22] G. K. Fleming and W. J. Koros, Macromolecules **19**, 2285 (1986).

[23] E.B. Zhulina, V.A. Borisov, and T.M. Birshtein, Macromolecules **24**, 140 (1991); S. T. Milner, T. A. Witten, and M. E. Cates, Macromolecules **21**, 2160 (1988).

[24] A. Karim, S. K. Satija, J.F. Douglas, J.F. Ankner, and L. J. Fetters, Phy. Rev. Lett. **73**, 3407 (1994).

[25] T. Morita, K. Kusano, H. Ochiai, K. Saitow, and K. Nishikawa, J. Chem. Phys. **112**, 4203 (2000).

[26] B. A. Younglove and J. F. Ely, J. Phys. Chem. Ref. Data **16**, 577 (1987).

[27] F.H. Huang, M. H. Li, K. E. Starling, and F. T. H. Chung, J. Chem. Eng. Jpn. **18**, 490 (1985).

[28] T. P. Russell, Mater. Sci. Rep. **5**, 171 (1990).

[29] *The International Technology Roadmap for Semiconductors*. (2001).

[30] S. L. Xu, J. H. Lee, J. J. Kim, H. Y. Lee, and S. H. Cho, Materials Science and Engineering B-Solid State Materials for Advanced Technology **99** (1-3), 483 (2003).

CHAPTER III

Introduction of Molecular Scale Porosity into Semicrystalline Polymer Thin Films Using Supercritical Carbon Dioxide

Appl. Phys. Lett. **94**, 121908 (2009)

Abstract:

We report supercritical carbon dioxide ($scCO_2$) technology used for forming a large degree of molecular scale porosity in semicrystalline polymer thin films. The following three steps were integrated: (i) pre-exposure to an organic solvent which melted crystalline structures, but did not cause a decrease in thickness, (ii) $scCO_2$ exposure under the unique conditions where the anomalous absorption of CO_2 occurred, and (iii) subsequent quick evaporation of CO_2 to preserve the swollen structures. This unified process resulted in homogenous low-density poly-phenylene vinylene films (a 15% reduction in density) with sustained structure for at least 6 months at room temperature.

3.1 Introduction

Porous polymer thin films have received great attention for many industrial applications such as tissue engineering, drug delivery, higher performance integrated circuit designs, fabricating chromatographic materials, and serving as catalysts in chemical and biochemical reactions[1]. During the last two decades, extensive studies have been made towards creating porous structures in glassy polymers using supercritical carbon dioxide ($scCO_2$, T_c = 31.3 °C and P_c = 7.38 MPa) as an environmentally benign solvent[2]. These procedures commonly rely on the same principles: (1) a polymer is saturated with $scCO_2$, which plasticizes the matrix and lowers the effective glass transition temperature to near room temperature, (2) the polymer/CO_2 mixture is then quenched into a supersaturated state by either reducing pressure or increasing temperature, and (3) nucleation and growth of pores continues until vitrification occurs. As a result, porous materials with pore sizes typically in the range of 10 nm - 10 mm can be created[2]. However, for interdisciplinary applications such as filtration, gas separation, catalysts, and ion-exchangers, as well as for the fundamental understanding of confinement effects on phase separation and phase equilibria of fluids, the formation of "micropores" (< 2 nm) is crucial[3].

To this end, we recently established the formation of molecular scale porosity in amorphous polymer thin films using $scCO_2$[4]. The object of this paper aims to further extend the $scCO_2$ process to semicrystalline polymers, which are much more robust and resistant to degradation than amorphous polymers. However, the challenge is that the solubility of $scCO_2$ with semicrystalline polymers is typically poor due to the rigid crystalline structures that prevent CO_2 molecules from penetrating into a polymer matrix[5,6]. To overcome this difficulty, and meet the pore size demands, we developed an alternative method for forming micropores in semicrystalline polymers by integrating three strategies: (i) pre-exposure to an organic solvent

that facilitates the melting of crystalline structures, and then allows CO_2 molecules to fully penetrate and diffuse throughout the film; (ii) low-temperature $scCO_2$ exposure near the critical point, where the anomalous absorption of CO_2 molecules into various amorphous polymer thin films occurs due to the large density fluctuations of CO_2[7,8]; (iii) subsequent quick evaporation of CO_2 which allows us to preserve the expanded structures created in $scCO_2$ without the formation of nano-to-micron scale porosity[9]. In addition, by choosing an organic solvent that can be easily dissolved in $scCO_2$, the solvent can be completely removed from the film during the quick evaporation.

3.2 Experimental Section

The semicrystalline polymer used in this study was poly-phenylene vinylene (PPV, glass transition temperature (T_g) ~ 220 ºC). Due to inherent characteristics, such as its initial low dielectric constant (k = 2.6), high temperature stability (up to 450 °C in N_2 ambient), and easy film preparation, PPV is expected to be an ultralow-k material. PPV thin films were prepared via chemical vapor deposition (CVD) by vapor phase pyrolysis of a,a'-dibromo-*p*-xylene onto silicon wafers[10]. The conversion of the precursor film was performed by vacuum annealing at T = 250 °C for measured times (10 - 40 min). All experiments were initially performed on films with a measured thickness of approximately 40 nm. For the PPV films, toluene (≥ 95% A.C.S. reagent) was chosen as the pre-exposure solvent for its inability to dissolve PPV quickly, and its ability to dissolve in $scCO_2$ readily[11]. As will be discussed later, we found that the pre-exposure time of 1 h was adequate for our intentions. The films, after the pre-exposure, were then quickly placed into a high-pressure cell and exposed to $scCO_2$ for 24 h under the "density fluctuation

ridge" condition (T = 36 ºC and P = 8.2 MPa), and subsequently depressurized to atmospheric pressure within 10 s.

3.3 Results and Discussion

First, we demonstrate the validity of toluene as the pre-exposure solvent. A grazing incidence X-ray diffraction (GIXD) technique, which is sensitive to crystalline structures within a film, was utilized. The GIXD measurements were conducted at the x10B beamline of the National Synchrotron Light Source (NSLS), Brookhaven National Laboratory (BNL) using a photon energy of 14 keV, i.e., x-ray wavelength (λ) of 0.087 nm. Figure 3-1 shows the GIXD profiles before and after pre-exposure to toluene. The pre-exposure was carried out just prior to the GIXD experiments. The glancing angle of incidence was set to 0.2°, just above the critical angle of 0.14° for PPV, in order to determine the crystal structure within the entire film. Prior to immersion in toluene, we could see the multiple Bragg peaks assigned to (110), (210), (120), and (410) lattice planes, indicating the existence of the crystalline regimes within the film[12]. However, when the sample was pre-exposed to toluene, this definitive crystal structure was no longer recognizable in the GIXD profile, as shown in Fig. 3-1. In addition, ellipsometry results proved no changes in the film thickness before and after the pre-exposed process. It should be added that longer pre-exposure times of more than 3 h caused a slight decrease in the film thickness, indicating that the film was partially dissolved. Consequently, to melt the crystal structures completely and prevent any decrease in the film thickness, we set the pre-exposure time for the PPV films to be 1 h. Next, we discuss the effect of the unified process on the exposed PPV films by using X-ray reflectivity (XR) measurements performed at the same NSLS beamline. Fig. 3-2 (a) plots the density profiles for the as-prepared film without pre-exposure,

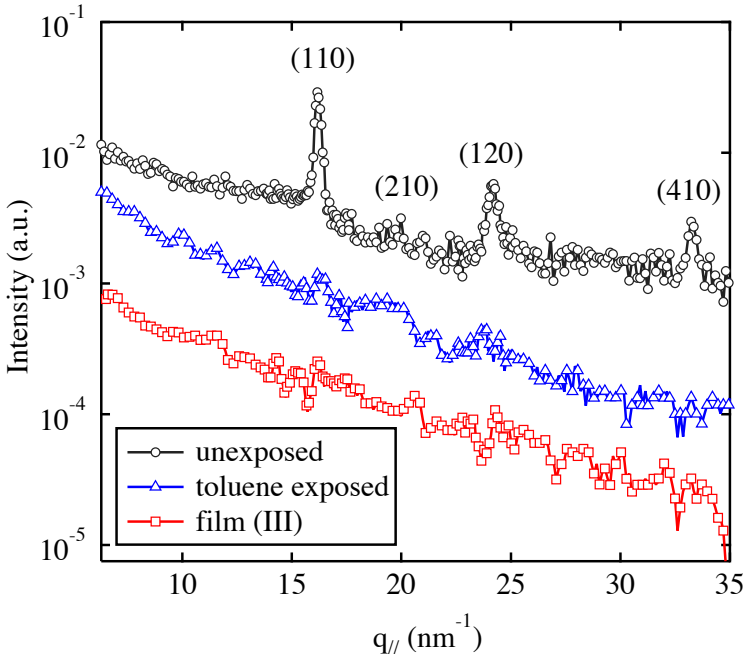

Figure 3-1. GID profiles for the PPV films without and with toluene exposure, and the film with toluene and $scCO_2$ exposure (III). The (HK0)s correspond to the miller indices for the PPV crystal structure.

hereafter defined as "film (I)", the film with exposure to only $scCO_2$, hereafter defined as "film (II)", and the film with the unified process, hereafter defined as "film (III)". Based on the Fourier Transform (FT) analysis method for XR developed by Seeck[13], we found that the film (II) was comprised of two layers with different densities. Hence, a four-layer model, i.e., a Si substrate, a SiO_2 layer and two PPV layers, was used to analyze the XR data for the film (II), while a three-layer model was used for the homogenous films (I) and (III). The dispersion (d) value in the x-ray refractive index, which is proportional to the density of a film, was obtained from the best-fits of the XR data and converted into the density of the film relative to the bulk by using the measured dispersion value of the untreated PPV film ($d = 1.34\times10^{-6}$). From to the film (II) measurements, the initial thickness, L_0 = 35.3 nm, has increased to L = 41.7 nm, which corresponds to a linear dilation, $S_f = (L-L_0)/L_0 = 0.18$. This value is much larger than the bulk swelling (= 0.07), indicating that the similar excess swelling described above occurred in the PPV film, and that the swollen structure could be frozen due to the vitrification. From the best-fits, we found that the expanded film became 15 % lower in density relative to the bulk. However, this low-density region occurred only at the surface area, approximately 20 nm depth, with a uniform layer of the bulk density beneath, and a relatively sharp interfacial width (2.0 ± 0.4 nm). On the other hand, it was found that the density of film (III) decreased by the same magnitude as film (II), 15%, but *throughout* the entirety film. Thus, it is clear that the pre-exposure, which melted the crystalline regime, enhanced the penetration power of $scCO_2$.

Furthermore, small-angle x-ray scattering (SAXS) experiments with reflection geometry[14] gave us pore-size distributions within the film (III). In order to avoid strong specular reflection, the sample position was slightly shifted with the angle of 0.1º from the symmetric $q/2q$ position (offset scan). The details have been described elsewhere[14]. Fig. 3-2(b) shows the observed

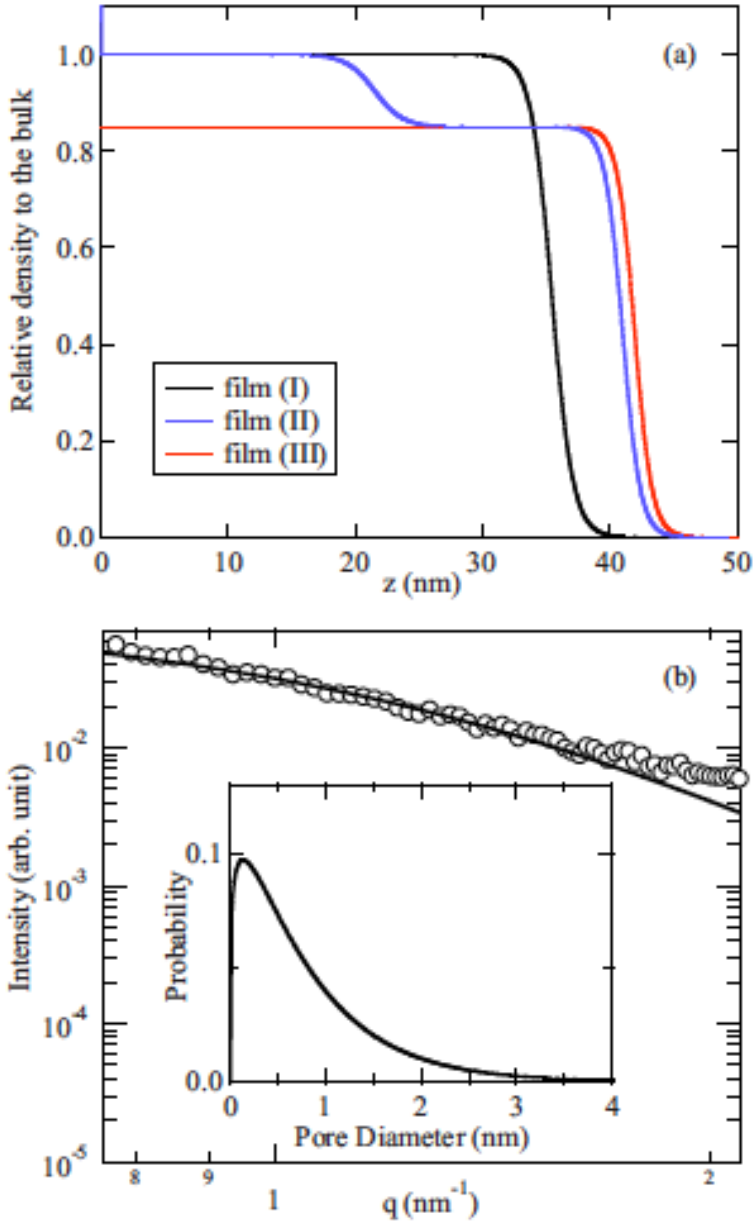

Figure 3-2. (a) Density profiles of the films (I), (II), and (III) obtained from the best-fits to the XR data. (b) Experimental (circles) and the best-fitted theoretical (solid line) SAXS profiles for film (III). In the inset, the pore-size distribution of the film with R_0=0.4 nm, M=1.2 using the 3-1 is plotted.

(circles) and calculated (solid line) SAXS profiles for the film (III). The observed SAXS profile was analyzed by comparison with the calculated SAXS profile based on the assumption that the pores had a spherical shape with a size distribution of a Γ-distribution mode:

$$I(q,R_0,M) = \frac{1}{\Gamma(M)}\left(\frac{M}{R_0}\right)^M \int_0^\infty e^{-M\times R/R_0} R^{M-1}\left(\frac{R_0}{R}\right)^3 [r_e\rho\bar{f}(q)\Omega(q,R)]^2 dR \qquad (3\text{-}1)$$

where $\Omega(q,R) = 4\pi R^3/(qR)^3(\sin(qR) - qR\cos(qR))$, r_e is the classical radius of electron, r is the number density of the atoms, and $\bar{f}(q)$ is the average atomic scattering factor of the film material, respectively. Note that the deviation between the observed and calculated SAXS profiles at $q > 1.7$ nm^{-1} may be attributed to the fact that the shape of the pores is not spherical but more elongated[15]. As shown in the inset of Fig. 3-2(b), the average size of the pores was estimated to be 0.8 nm with a relatively broad size distribution. Hence, the XR and SAXS techniques led to the important conclusion that the unified process could introduce a large degree of molecular scale porosity into the entire film, resulting in the low-density film formation. In addition, XR experiments also clarified that the film (III) was stable for at least 6 months at room temperature, allowing for further subsequent processing. So far, the unified process offers to produce homogenous PPV films up to 80 nm thickness with further optimization of the conditions currently in progress.

Finally, we discuss the physical and thermal properties of the homogenous low-density PPV film. It is known that a reduction in density of an amorphous polymer is associated with a reduction in index of refraction (n). As shown in Fig.3-1, we confirmed that the low-density PPV film (III) did not have any crystalline structures within the film. By using a VASE Research Spectroscopic Ellipsometer (M-44, J.A. Wollam Co, Lincoln, NE) based on a biaxial Cauchy

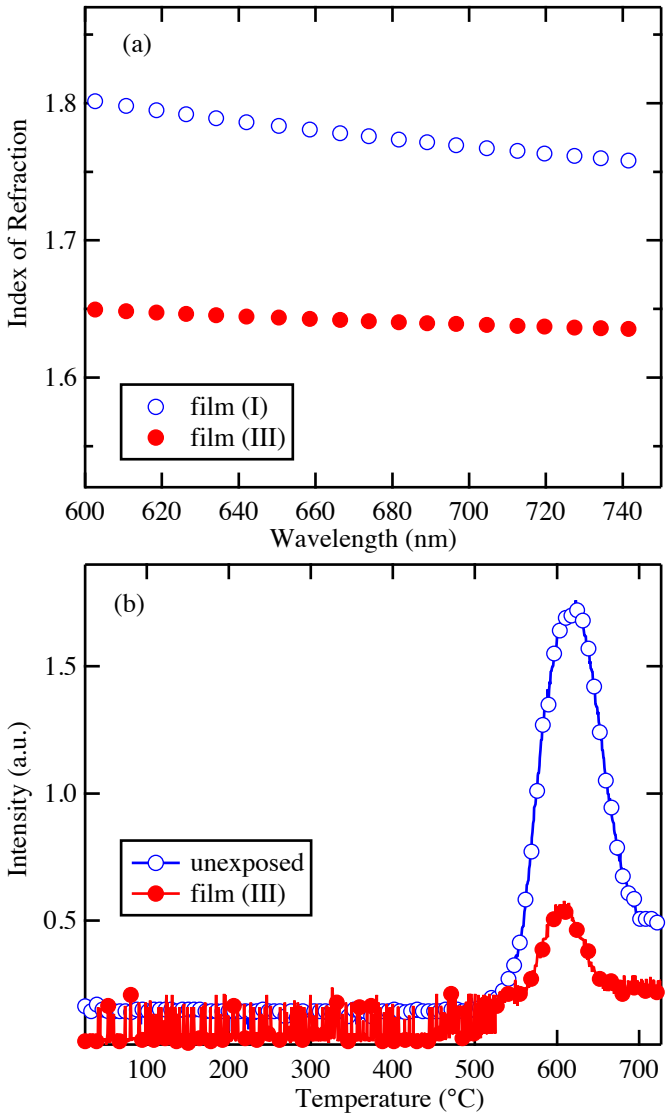

Figure 3-3. (a) Index of refraction vs. wavelength for the film before (red) and after $scCO_2$ treatment (blue). (b) Continuous mass spectra of toluene fragment mass taken during temperature ramping are shown. Note that the untreated sample exhibits the higher intensity because of the larger initial thickness of the prepared film **(**65 nm**)**.

model, we measured the change in the optical property. In order to fit the data, the same three-layer model used for the XR analysis was utilized with the literature *n* values for a SiO_2 layer and Si substrate. Since the film thicknesses of both PPV and SiO_2 layers could be determined by XR, the only floating parameter was the *n* value of the PPV layer. Figure 3-3(a) shows the indices of refraction for the films (I) and (III). From the figure we can see that there is a significant decrease (about 8 %) in *n* for the film (III) over the entire range of the wavelength (600 nm – 742 nm). Based on the Lorentz-Lorentz equation, $(n_a^2 - 1)/(n_a^2 + 2) = (1 - v)(n_b^2 - 1)/(n_b^2 + 2)$[16], where n_a and n_b are the refractive indices of the exposed and unexposed films, respectively, and *v* is a volume fraction of porosity, the porosity was estimated to be 13.8 ± 0.5 %. This number is in good agreement with the decrease in the density obtained by the XR data. Interestingly, this change in *n* corresponds to an about 15% decrease in *k* if the well-known relationship of $k \sim n^2$ is valid.

The thermal degradation property of the film (III) was also studied by means of *in situ* Mass spectroscopy using MILA-3000 mini lamp cold wall annealing system (ULVAC/Sinku-Riko Inc., Chigasaki, Japan) connected to a differentially pumped Residual Gas Analyzer RGA-300 (Stanford Research Systems Inc., Sunnyvale, CA)[10]. Figure 3-3(b) shows the spectra for the unexposed film and film (III) taken during dynamic heating at a rate of 20 ºC/min up to 800 ºC. A large peak in intensity indicates the release of significant amounts of toluene ($C_7H_7^+$) owing to the film degradation[10]. Thus, the peak initiation (approximately at 500 ºC) remains unchanged before and after the unified process, proving that the low-density film (III) still imparts the high thermal stability inherent to the material.

3.4 Conclusions

In conclusion, with the unified methodology using an organic solvent in conjunction with supercritical carbon dioxide, we could introduce a large degree of molecular scale porosity into semicrystalline PPV films. The resultant “microporous” film showed significant reductions in the density-dependent properties, while maintaining the structure for at least 6 months at room temperature and the high performance thermal property.

3.5 References

[1] P.J. Langley and J. Hulliger, Chem. Soc. Rev. **28**, 279 (1999).

[2] A. Cooper, J. Mater. Chem. **10**, 207 (2000).

[3] L.D. Gelb, K.E. Gubbins, R. Radhakrishnan, M. Sliwinska-Bartkowiak, Rep. Prog. Phys. **62,** 1573 (1999).

[4] T. Koga, J. Jerome, M. H. Rafailovich, B. Chu, J. Douglas, and S. Satija, Adv. Coll. Interf. Sci. **128**, 217 (2006).

[5] E. Weidner, V. Wiesmet, Z. Knez, and M. Skerget, J. of Supercrit. Fluids **10**, 139 (1997).

[6] Y. Li, E. J. Park, K. T. L. Lim, K. P. Johnston, and P. F. Green, J. Polym. Sci. Part B: Polym. Phys. **45**, 1313 (2007).

[7] T. Koga, Y. S. Seo, Y. M. Zhang, K. Shin, K. Kusano, K. Nishikawa, M. H. Rafailovich, J. C. Sokolov, B. Chu, D. Peiffer, R. Occhiogrosso, and S. K. Satija, Phys. Rev. Lett. **89**, 125506 (2002).

[8] T. Koga, Y. S. Seo, K. Shin, Y. Zhang, M. H. Rafailovich, J. C. Sokolov, B. Chu, and S. K. Satija, Macromolecules **36**, 5236 (2003).

[9] T. Koga, Y. S. Seo, J. L. Jerome, S. Ge, M. H. Rafailovich, J. C. Sokolov, B. Chu, O. H. Seeck, M. Tolan, and R. Kolb, Appl. Phys. Lett. **83**, 4309 (2003).

[10] C. A. Gedelian, G. A. Ten Eyck, and T. M. Lu, Synth. Met. **157**, 48 (2007).

[11] J. Fang and E. Kiran, Macromolecules **41** (20), 7525-7535 (2008).

[12] G. Mao, J. E. Fischer, F. E. Karasz, and M. J. Winokur, J. Chem. Phys. **98**, 712 (1993).

[13] O. H. Seeck, I. D. Kaendler, M. Tolan, K. Shin, M. H. Rafailovich, J. Sokolov, and R. Kolb, Appl. Phys. Lett., **75**, 2713 (2000).

[14] K. Omote, Y. Ito, and S. Kawamura, Appl. Phys. Lett. **82**, 544 (2003).

[15] See, for example, A. Guinier and G. Fournet, *Small-Angle Scattering of X-rays* (John Wiley & Sons, London, 1955).

[16] M. Born, and E. Wolf, *In Principles of Optics*; Cambridge University Press: Cambridge, UK, 1999.

CHAPTER IV:

New insight into the formation of an irreversibly adsorbed polymer layer at the impenetrable interface

Abstract:

Using experimental techniques, we have investigated the structure and formation of the irreversibly adsorbed polymer layer from a melt onto a solid interface. For polystyrene (PS) it was found that near the solid wall, a higher than bulk density (approximately 20%) flattened layer of 3.5 ± 0.5 nm in thickness formed regardless of the molecular weights. At the same time, an outer layer, which is unable to fully penetrate and contact with the solid, loosely attaches at the solid and exhibits a random coil configuration near the free surface. It was found that the adsorbed polymer layer expressed significantly reduced swelling behavior and suppressed dynamics in density fluctuating supercritical carbon dioxide relative to the ultrathin film and brush cases. Subsequent application of a good solvent after $scCO_2$ processing leeched away the loosely attached outer layer and ultimately revealed the thermodynamically stable flattened inner layer.

4.1 Introduction

The adsorption of polymer chains onto a solid has been often described as irreversible when a large number of chain segments (N) attach to strongly attractive surface[1, 2]. As a result, the inhibition of segmental mobility from melts or solutions has been linked to observed deviations from bulk polymer behavior[3]. For example, perturbations in viscosity[4], diffusivity[5], thermal expansivity[6], and glass transition temperature (Tg) [3, 7] have been shown to persist in thin films up to several R_g[5, 8, 9] (where R_g is the polymer radius of gyration). It has been suggested that the formation and consequently the deviations from bulk behavior originate from the impenetrable interface.

Theoretical studies of the equilibrium structure of polymer chains reversibly adsorbed from a dilute solution have been presented in the classical study by de Gennes[10]. In a good solvent, the structure of equilibrium-adsorbed layer is independent of the bulk concentration, taking on a self-similar structure, whereby most of the monomers are confined within a small region. However, experimental ellipsometric and neutron reflectivity studies found that the adsorbed layer thickness increased with molecular weight[11, 12]. More recent studies by Semenov et al.[13] have suggested a more complex configuration than the classical study. When the bulk solution is dilute, the adsorbed polymer layer has a dual layer structure with an inner layer dominated by loops and an outer layer dominated by tails. The tails of the chains are expelled from the region close to the adsorbing wall leading to an increase of concentration away from the wall, which explains the thickening of the adsorbed layer. O'Shaughnessy and Vavylonis[14, 15] theorized, at the initial stages of layer formation from a dilute solution, the surface is almost empty and the first chains to arrive, via a simple random walk, adsorb on the surface without interference from others. At longer times, a polymer layer of strongly interacting chains develops and chain

densities on the surface become much higher than those in the bulk. For a semi-dilute solution, Semenov predicts a very similar formation to those of the dilute solutions[13]. However, there is a slight difference in the distribution of free chains. In this case, the adsorbed layer acts as an effectively impenetrable wall for free chains. Zajac and Chakrabati[9] recently proposed the formation from a dense solution is as follows: first loops on chains initially in contact with the surface in the solution, collapse onto the surface to fill empty sites when thermally annealed above T_g. Then, unattached chains diffuse to the substrate to reach unoccupied sites for adsorption. Similarly, Guiselin[16] has discussed the irreversible adsorption of polymer chains from a melt in detail. Rather surprisingly, recent studies have shown that the adsorbed polymer layer forms not only on an attractive substrate but also in weakly attractive[11, 17] and even non-attractive/repulsive[18, 19] polymer-substrate systems. Moreover, these studies have also reported similar deviations in viscosity, and Tg. Experimental evidence shows a relatively flat adsorption layer rather than the broad interface due to the stretched tail configuration as theoretically predicted.

Interfaces between polymers and hard materials (the so-called "soft-hard matter interfaces") play crucial roles in a multidisciplinary field of nanotechnology at the confluence of physics, chemistry, biology, and engineering. Nevertheless, comprehensive understanding of the structures/dynamics at the soft-hard interface is very challenging for both experimental and theoretical studies, because of the wide ranges of relevant length, time, and energy scales inherent to polymers. Therefore, our goals in this study are to provide detailed experimental descriptions of the structures and formation process of layers adsorbed from a melt onto smooth, flat solids under well-controlled contacting conditions, and to help bridge the theoretical and experimental viewpoints. Certainly, answering this underpinning problem can directly impact the

practical uses of nanotechnology in a wide variety of fields. In addition, we extend our experimental study to explore the effects of supercritical carbon dioxide ($scCO_2$) on the structures and dynamics of the adsorbed layer. The novel characteristics of $scCO_2$ as a solvent unfold the mechanism of the unique adsorption process at the soft-hard matter interface.

4.2 Experimental Section

Seven different molecular weights (M_w) of hydrogenated polystyrene (h-PS) (30×10^3, 50×10^3, 123×10^3, 170×10^3, 290×10^3, 650×10^3, and 2000×10^3) were obtained from Polymer Laboratories Inc. (Amherst, MA). The polydispersity indices (M_w/M_n) were less than 1.2. Samples of varying M_w h-PS were prepared from toluene (Sigma-Aldrich, ACS reagent, > 99.5%) solutions onto hydrogen-passivated silicon (H-Si) substrates, where a native oxide layer was removed by submerging them in an aqueous solution of hydrofluoric acid, and subsequently annealed at 150 °C for at least 48 h in an oil free vacuum below 10^{-3} Torr. The initial thicknesses of the as cast films were approximately 60 nm. The adsorbed layers were then revealed by thoroughly submerging and rinsing the samples in toluene. The removal procedure was repeated until the thicknesses of the residual layer, evaluated by spectroscopic ellipsometry (Rudolph Electronics, AutoEL-II), were constant. The adsorbed films were further annealed to remove any excess solvent trapped in the film before x-ray reflectivity experiments. X-ray reflectivity performed at the X10B beamline at the National Synchrotron Light Source, Brookhaven National Laboratory, was used to evaluate the density profiles of the adsorbed films normal to the surface. The photon energy of the beam was 14.1 keV (i.e., the x-ray wavelength (λ_x) of 0.087 nm). The specular reflectivity is measured at different incident angles and displayed as a function of the scattering vector in the perpendicular direction, $q_z = (4\pi\sin q)/l_x$, where q is the

incident angle. The XR data was fit using a standard multilayer fitting routine for a dispersion value in the x-ray refractive index along with a Fourier transformation (FT) analysis[20], which is a powerful tool to obtain detailed structures for low x-ray contrast multilayers. The dispersion (d) value in the x-ray refractive index, which is proportional to the density of a film, was obtained from the best-fits of the XR data and then converted into the density of the film relative to the bulk by using the measured dispersion value of the untreated or bulk PS film ($d = 1.14\times10^{-6}$) with the x-ray energy.

In-situ specular neutron reflectivity (NR) measurements were performed on the NG7 neutron reflection spectrometer at the National Institute of Standards and Technology (NIST) with a wavelength (λ_N) of 0.47 nm and a $\Delta\lambda/\lambda$ of 2.5 %. Details of the high-pressure cell used for NR measurements have been described elsewhere[21]. The temperature of the system was controlled with an accuracy of ± 0.1°C and the stability of each pressure during the measurements was less than ± 0.2 %. An adsorbed layer composed of deuterated PS (d-PS, $M_w = 690\times10^3$) was prepared on 8 mm thick Si wafers with a 3-inch diameter for the experiments. The thickness of the adsorbed layer in air was determined to be 12 ± 0.5 nm in the dry state by using NR. CO_2 was then injected into the high-pressure cell containing the film and pressurized to predetermined values at isothermal conditions (T = 36 °C) for the reflectivity measurements. The films were exposed to CO_2 for up to 1 h prior to data acquisition in order to ensure that the equilibrium swelling was achieved. Data was obtained both by successively increasing the pressure and then slowly decreasing the pressure. The results were identical, indicating that all the swelling isotherms were reversible with pressure and temperature. Since the background scattering from a pure CO_2 phase increased dramatically near the critical points (density fluctuations), we measured the scattering from the pure fluid phase for each pressure condition as background.

The NR data corrected for the background scattering was analyzed by comparing the observed reflectivities with the calculated ones based on model scattering length density (SLD) profiles. Fits of reflectivity from the adsorbed layer were obtained using a single "box" model. The values for scattering length density for the Si substrate were fixed based on published values (2.11×10^{-6} $Å^{-2}$). Values for the $SLD_{polymer}$, root-mean-square (rms) roughness (σ) at the interfaces (Si/polymer and polymer/free surface), and thickness of the film were optimized to achieve the best fits. Since the observed *q*-range used in this study is limited due to the large scattering intensity associated with the density fluctuations of the fluid, we used a single polymer layer model to fit the data. To measure the dynamics of the adsorbed layer composed of h-PS with different molecular weights, an additional layer of d-PS ($M_w = 333 \times 10^3$) was overlaid onto the adsorbed h-PS layers. The d-PS top layers were initially spun onto 4-inch diameter Si wafers with UV/ozone grown oxide layers to enhance the substrate's hydrophilicity. The d-PS films were subsequently removed from the non-attractive substrate by floating in a deionized water bath. The bilayer samples were dried at room temperature under vacuum for at least 18 h to ensure all traces of water were removed.

4.3 Results and Discussion

4.3.1 Structures of the irreversibly adsorbed polymer layer

Fig.4-1 (a) shows the time growth thickness (h_{ads}) of a representative adsorbed h-PS layer (Mw $=123 \times 10^3$) measured by XR. Napolitano et al. introduce a new criterion to define equilibrium of the conformation of polymer chains prepared on solid substrates, connected to the degree of adsorption, via the ratio *t** between the annealing time and the adsorption time. The adsorption

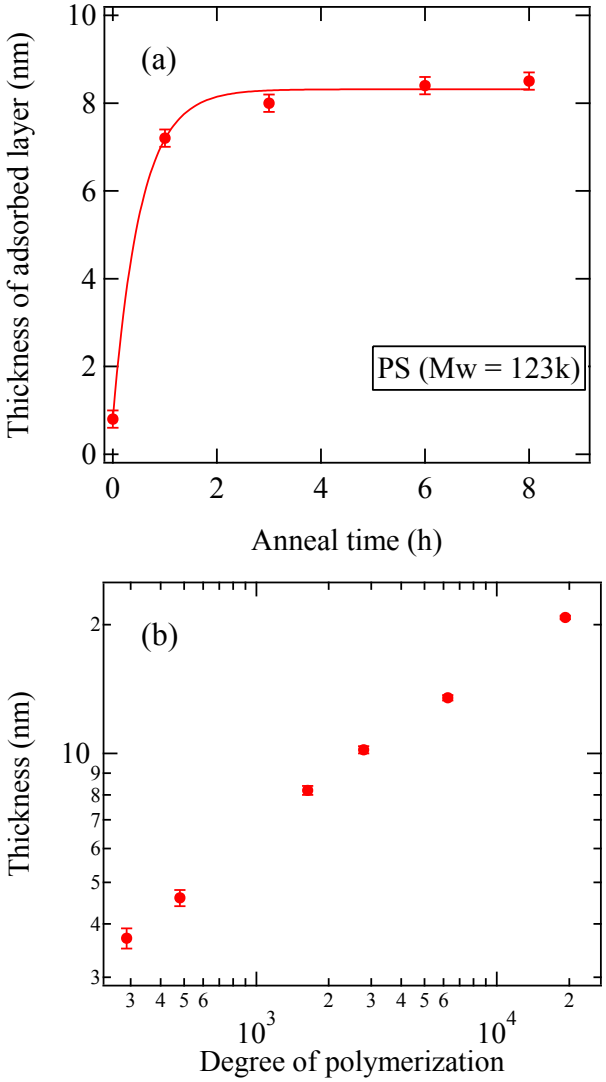

Figure 4-1. (a) Time evolution growth of adsorbed h-PS (Mw =123k) prepared by annealing at 150 °C (b) equilibrium thicknesses of the adsorbed layers as a function of the degree of polymerization

time (t_{ads}) can be estimated to be t_{ads} ~ 0.6 h based on the best-fit of the proposed function, $h_{abs}(t) \sim 1 - \exp(-t / t_{ads})$ to the experimental growth curve. In this case, thermodynamic equilibrium, which does not always correspond to the bulk behavior, is identified at $t^* >> 1$. Therefore the ratio t* is calculated to be 24h/0.6h =40 so that our annealing condition has met the criterion for equilibrium. It should be noted that all the t_{ads} values for the dead layers composed of different molecular weights are within 24 h. In addition, for all molecular weights used in this study, we found that a very thin adsorbed layer of 0.8 ± 0.1 nm in thickness and the surface coverage of 0.57 formed immediately after spin-casting from a toluene solution (0.015 g/ml) without subsequent annealing. Hence, it is clear that a large number of adsorption sites are not immediately covered with polymer chains after initial contact, resulting in the formation of the very thin layer, as seen in the PMMA adsorbed layer on quartz[12].

Figure 4-1 (b) shows a log-log plot of the thickness (h_{dry}) of the adsorbed layers in a dry state against the degree of polymerization and the segment length. A regression analysis of the data gives the scaling $h_{dry} \propto N^{0.49 \pm 0.04}$. This scaling of $h_{dry} \sim N^{1/2}$ reflects random-walk statistics of a polymer chain with N segments near a flat solid surface and is in good agreement with previous experimental results on h-PS adsorbed layers prepared on H-Si substrates[11] as well as PMMA adsorbed layers on quartz surfaces[12]. It should be added that the adsorbed films were further examined using atomic force microscopy, demonstrating a homogenous surface, free of noticeable voids or defects, as seen in Figure 4-2.

Figure 4-3 (a) shows representative XR profiles (h-PS, Mw = 123×10^3) with their respective best fits to the calculated reflectivity profiles based on a four-layer model, i.e., silicon substrate, the native oxide and two PS layers with different densities. For comparison, we also plot the

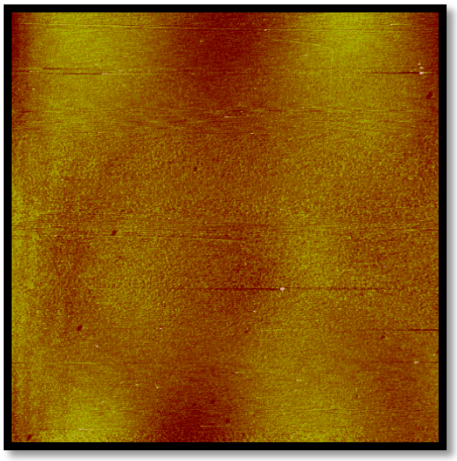

Figure 4-2 Representative (PS Mw = 123 k) height mode AFM image of the equilibrium adsorbed layer after removing unbound polymer.

best-fits based on the three-layer model (i.e., a single homogenous h-PS layer on top of the native oxide). From the figure we can see the four-layer model expresses the XR profile more accurately over the q-range used. The thickness of a silicon oxide layer was determined to be about 1.0 nm from XR experiments for a bare H-Si substrate. Figure 4-3(b) shows the density profiles obtained from the best-fits. Interestingly, we found that all of the films exhibit a thin-higher (20 percent higher than the bulk) density region (about 4 nm in thickness) near the substrate, while the density near the air/polymer interface remains almost bulk-like. This may be consistent with the picture developed by Granick and coworkers for polymer adsorption from a dilute solution: early-arriving polymer chains lie flat on the substrate, while late arriving ones, which find less free surface area, adsorb more loosely with fewer adsorbed sites, i.e., "lesser footprint"[17, 22-24]. The formation of the higher density layer near the substrate has been previously observed using neutron reflectivity for the adsorbed PMMA layer on quartz[12] as well as d-PMMA annealed on glass[25] prepared by spin-casting. Although this disagrees with Wu et al. who reported that the density of very thin films of d-PS and d-PMMA (annealed at 90 °C for 1h) are less than those of the bulk[26], recent XR experiments by Kanaya and co-workers[27] indicate that this low-density formation may be due to a result of insufficient annealing time necessary to erase the effect of the solvent for spin-cast films.

4.3.2 Formation Mechanism of the irreversibly adsorbed polymer layer.

To get a better understanding of the formation mechanism, we also characterized the transient structures of the adsorbed layer prior to equilibrium using AFM and XR. Samples for this formation time dependence study were prepared by thermal annealing in vacuum at 150 °C for

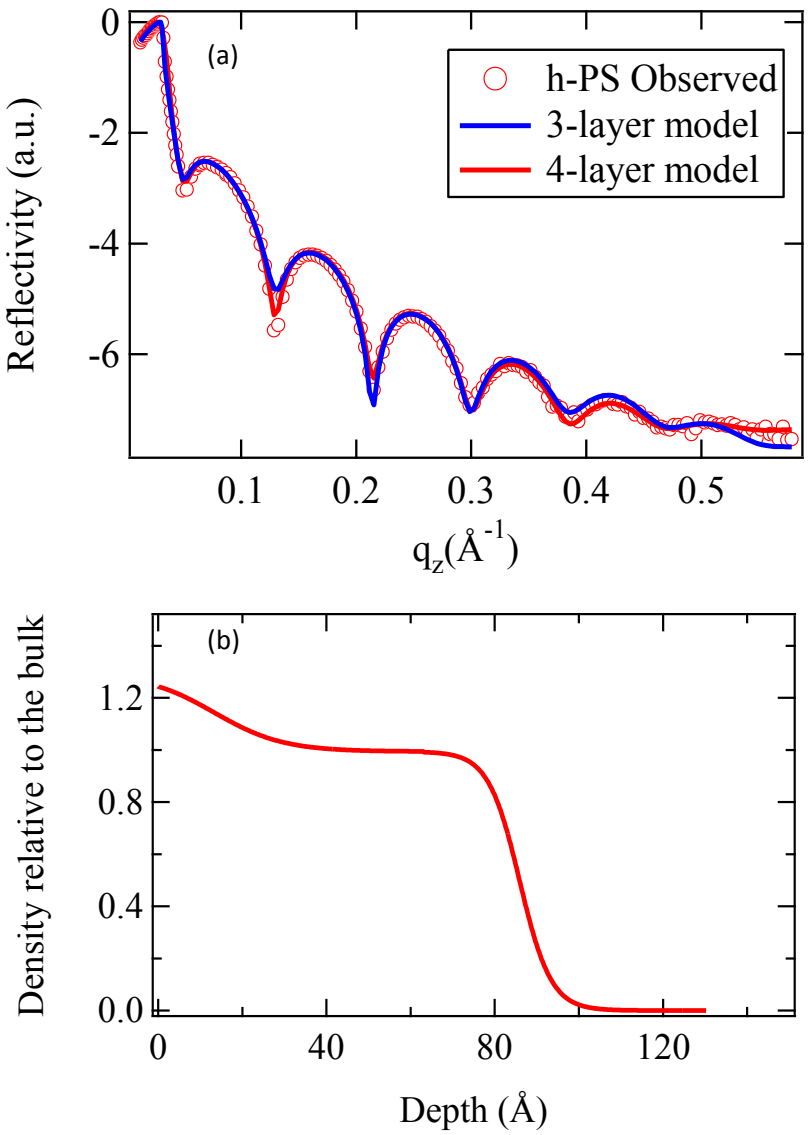

Figure 4-3. (a) Observed (circles) XR profiles for h-PS (Mw =123k) plotted with the best calculated fits (line) based on the 3 and 4-layer models (b) density profile as a function of the distance from the SiO_2 surface extracted from the best fits.

predetermined times and subsequently removing the unattached polymer using the previously discussed leaching method. Figure 4-4 shows representative height mode images of the adsorbed

PS layer ($M_w = 123 \times 10^3$) for different annealing times (1h, 3h, and 8h). It is clear that for short times (t < 3h), the layer is heterogeneous and does not fully cover the substrate surface. However, as the annealing time is increased, we can see improvements in the surface coverage,

and after 8 h a relatively smooth, homogenous layer is achieved. It is important to point out that the corresponding friction images (data is not shown here) for the shorter annealing times demonstrate that there are no differences in surface hardness between the dark (i.e., lower heights) and bright areas (higher heights) of the height image, proving that the substrate surfaces are fully covered with the polymer layers, but composed of different heights (In fact, the cross-sectional AFM profiles estimate the vertical distance between the valley and peaks to be about 6 nm for 1 h and 5 nm for 3 h). In order to further characterize the heterogeneous film structures, XR was utilized. Figure 4-5 shows the observed and calculated XR curves based on the four-layer models. The fitting results are summarized in Table 4-1. Note

Annealing time (h)	*Top δ (x 10^{-6})*	*Bottom δ (x 10^{-6})*	*Top h (nm)*	*Bottom h (nm)*
1	0.97±0.03	0.97±0.03	6.0±0.1	1.0±0.1
3	1.05±0.03	1.3±0.03	6.2±0.1	1.7±0.1
8	1.16±0.03	1.26±0.03	4.4±0.1	4.0±0.1

Table 4-1. Dispersion (δ) and thickness (h) values obtained from the calculated best fits of XR profiles the transient after annealing at 150 °C.

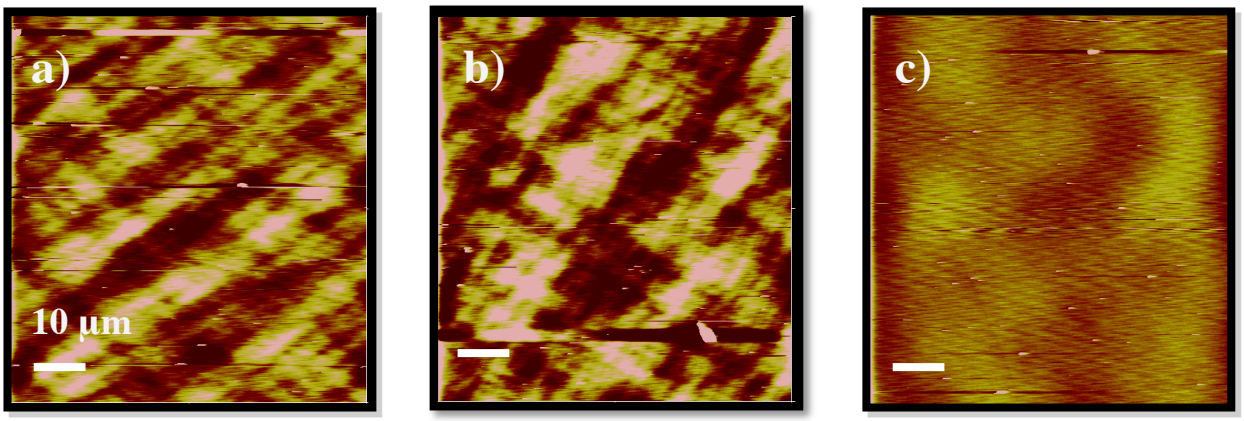

Figure 4-4. Height-mode AFM images of the adsorbed PS (Mw = 123k) transient structures after annealing for (a) 1 h (b) 3h and (c) 8 h at 150 °C.

that the δ value of bulk PS is 1.14×10^{-6}. These XR results elucidate how the aforementioned top (bulk-like) and bottom (higher density) layers are formed in the course of the annealing process. Although the thickness of the adsorbed layer formed after the annealing time of 1h is almost identical (7.2 nm) to the equilibrium one (8.4 nm), the difference in δ between the top and bottom layer is not clear. At t=3 h, the bottom layer densified beyond the bulk value and the formation of the two layers is easily differentiated, while the density of the top layer is still lower than the bulk value. We found that the annealing time of 6 h at T=150 °C is required to form the equilibrium layer structures. These results show that at the initial stage of the adsorption process, the substrate surface is partially covered with the polymer chains, while the thickness of the layer is nearly equivalent to the equilibrium thickness. When further annealed, the coverage increases until essentially all attached chains have fully adsorbed and a monolayer of flattened chains starts to develop. During the final stage of the adsorption process, the growth of the layer is dominated by a "reeling in" of the partially adsorbed late-coming chains, which becomes complicated for large chain lengths, resulting in unexpectedly long relaxation modes as indicated by Napolitano et al.[3].

4.3.3 Effect of $scCO_2$ on the irreversibly adsorbed polymer layer.

The next question to be addressed is how swollen is the adsorbed layer in a solvent? According to Durning et al.[12], who prepared adsorbed PMMA layers on quartz substrates using a similar protocol, the adsorbed layers exhibited highly extended structures in deuterated benzene (a good solvent for PMMA) and are consistent with a power-law profile $\phi(z) \propto z^{-\alpha}$ (a~0.8). At the

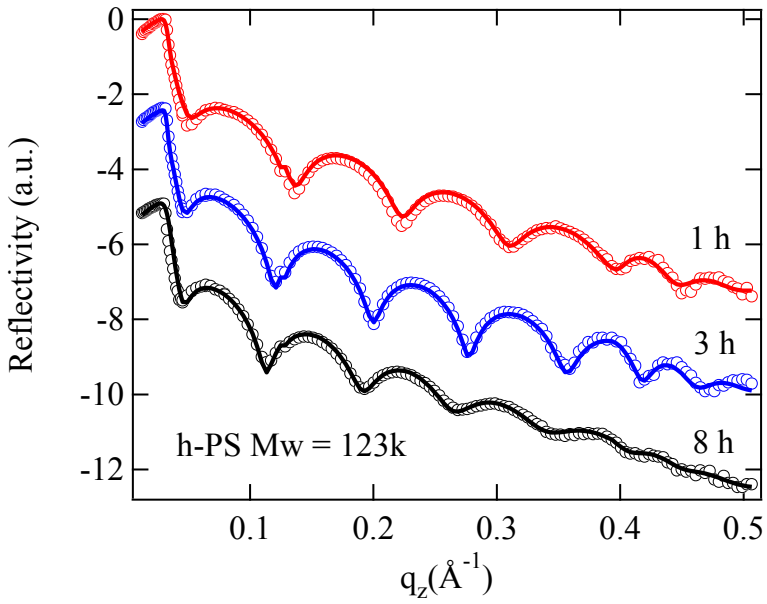

Figure 4-5. Observed XR profiles (circles) of the adsorbed PS (Mw =123k) after annealing at 150 °C for 1, 3, and 8 h. The solid lines represent the corresponding best fits.

same time, their data suggests the presence of the less swollen layer (the volume fraction of the polymer is close to nearly 1) within 2 nm of the quartz surface, possibly the formation of a flattened layer, but the authors never mention it. In this study, we chose supercritical carbon dioxide ($scCO_2$) as a solvent for the PS adsorbed layers because of the following novel characteristics: (i) Enhancement of CO_2 absorption into PS thin films near the critical point, resulting in anomalous expansion of the polymer chains[21, 28,29] and the corresponding plasticization effects[21, 30]; (ii) PS thin films can be vitrified when the fluid is released rapidly, and the swollen structures can be preserved as they are in CO_2[30], allowing us to further characterize the swollen structures in air. This depressurization process is known to form micron scale porous structures in bulk polymers[31, 32]. However, in cases of polymer thin films, it is found that the average size of pores formed in the frozen glassy polymer films is less than 1 nm (i.e., molecular scale porosity) [33].

The observed neutron reflectivity profiles from the adsorbed d-PS ($M_w = 690\times10^3$) layer in the presence of CO_2 along with their corresponding best fits can be seen in Figure 4-6(a). The thicknesses determined from the best fits were used to calculate the swelling ratios of the adsorbed film, $S_f = L_1\text{-}L_0/L_0$, where L_1 and L_0 are the measured thickness of the swollen and unswollen adsorbed layer, respectively. The results at T=36°C are shown in Figure 4-6(b) where we can see the adsorbed d-PS layer swells in CO_2, but the degree is rather small (at most 10%) within the pressure range used in this study. At the same time, a noticeable anomalous peak is present in S_f near the density fluctuation ridge (P_{ridge} = 8.2 MPa at T =36 °C for CO_2)[34] where excess swelling of ultrathin PS films[30] has occurred. It should be noted that the magnitude of the excess expansion of the adsorbed layer at the ridge is much less than that of PS ultrathin films or brushes ($S_f \sim 0.25$)[30]. This suppression in S_f suggests that the adsorbed layer does not have as

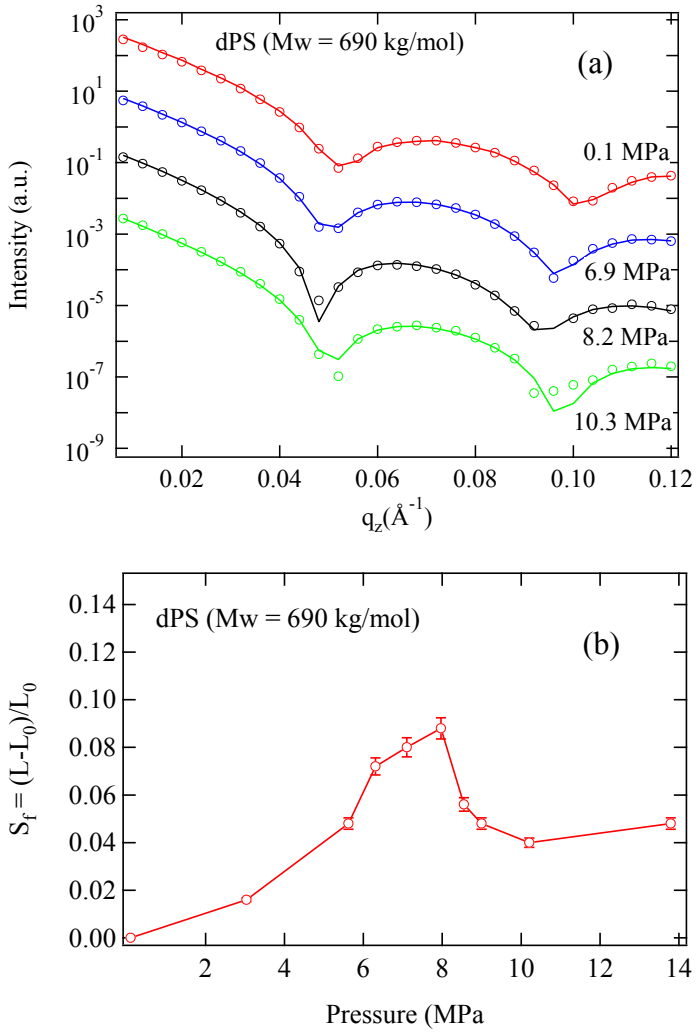

Figure 4-6. (a) Representative NR profiles (circles) and the corresponding best fits (line) of d-PS (Mw = 690k) at predetermined pressures under isothermal conditions (T =36°C) (b) Pressure dependence of the swelling ratios calculated from the best fits of the observed NR profiles.

many "tails" as polymer ultrathin films (the so-called "Guiselin brushes"[16]) or brushes. It should be noted that detailed analysis on the density profile of the swollen adsorbed layer in $scCO_2$ was not possible due to the limited *q*-resolution ($q_{max} = 0.13Å^{-1}$) caused by large scattering intensity of CO_2 (i.e., the long-range density fluctuations near the critical point[35]) as a source of background.

Following the $scCO_2$ exposure for 2 h at the ridge condition and depressurized quickly (within 10 s) to atmospheric pressure, the swollen adsorbed layers were further rinsed with toluene to see whether the adsorbed layers remain unchanged. Interestingly, we found that the unified process of the $scCO_2$ exposure followed by the toluene leaching results in a further decrease in the film thickness relative to the one prior to the $scCO_2$ treatment. Figure 4-7 summarizes the changes in the thickness of the absorbed layers determined by XR after the continued unified processes. Hence we can see all the adsorbed layers reached the equilibrium thickness of 3.5±0.5 nm and the dispersion value of $d = 1.30 \pm 0.1 \times 10^{-6}$ after several unified cycles regardless of the molecular weights (see, Table 4-2). It is interesting to point out that the density and thickness of this equilibrated adsorbed layer is in good agreement with larger-than-bulk density layer near the substrate observed in the unswollen adsorbed film (see, Fig. 4-3). These findings suggest that the

Mw (x 10^{-3})	123	170	290	650	2000
δ *(x 10^{-6})*	1.3±0.03	1.5±0.03	1.5±0.03	1.45±0.03	1.5±0.03
h (nm)	3.8±0.1	3.1±0.1	3.0±0.1	3.9±0.1	4.0±0.1

Table 4-2. Dispersion (δ) and thickness (h) values obtained from the best fits of the XR of the remaining equilibrium layer after repeat cycles of the unified process.

Mw (x 10^{-3})	123	170	290	650	2000
δ *(x 10^{-6})*	1.08±0.03	1.18±0.03	1.2±0.03	1.12±0.03	1.12±0.03
h (nm)	5.8±0.1	4.8±0.1	5.3±0.1	5.9±0.1	6.2±0.1

Table 4-3. Dispersion (δ) and thickness (h) values obtained from the best fits of the XR of the swollen equilibrium layer after $scCO_2$ captured by quick depressurization.

unified process removes the outer layer, resulting in the uncovering of the high-density flat layer.

The equilibrium flatten layers composed of different M_ws were further exposed to $scCO_2$ at the ridge for 2h, preserved via quick evaporation of CO_2, and characterized by XR. As summarized in Table 4-3, we found that the exposed flatten layers were expanded in the direction normal to = 150 °C for 2 h in vacuum after the XR experiments collapsed the swollen flatten films to the original thickness and density to the original value (i.e., 20% higher than the bulk) before the $scCO_2$ exposure. Consequently, we conclude that the more flattened conformation is thermodynamically favorable for the flatten chains in air due to the counterbalance between the entropy loss of the polymer chains adsorbed to the substrate and enthalpic contributions by increasing the numbers of monomer contacts with the attractive substrate.

It is known that the sticking energy (ε) for PS adsorbed on oxidized silicon is 1 k_BT/segment[36], which is relatively weak, compared to PMMA on oxidized silicon ($\varepsilon \approx 4k_BT$) due to hydrogen bonding. Given their chemical structures, it is not obvious how such short-range and strong bonds can be formed between PS and H-Si, even though H-Si is partially oxidized. According to a previous report, an absorbed layer of PS is also formed onto highly oxidized Si substrates, but

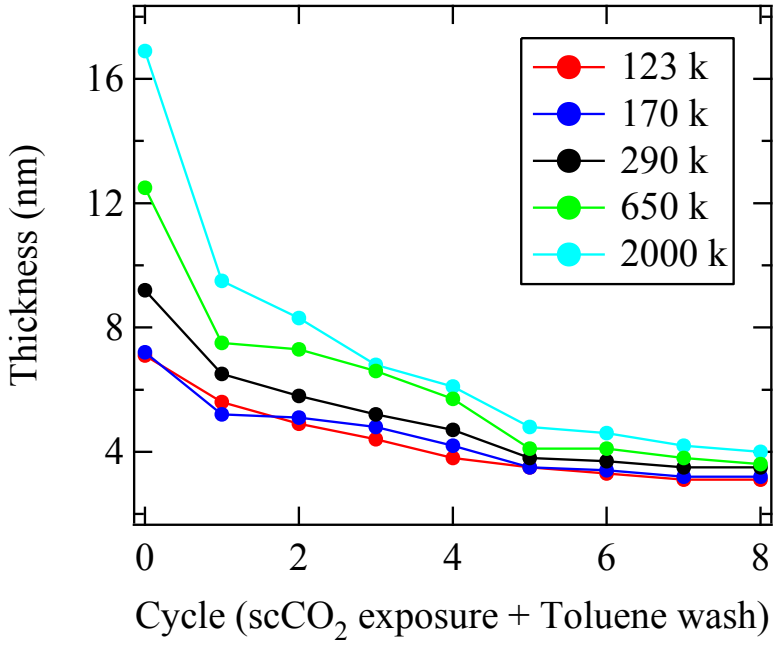

Figure 4-7. Thicknesses of the remaining adsorbed layer after cyclic removal of loosely attached polymer using the unified $scCO_2$ and good solvent treatment. Equilibrium is achieved after several cycles.

the thickness is much thinner (at most 1 nm) than those formed on H-Si substrates[11]. Hence, the sticking energy for PS/H-Si is expected to be larger than 1 k_BT. Recently, Bhattacharya et al. reported that the desorption mechanism of a polymer chain adsorbed on an attractive surface using a grand canonical ensemble approach[37]. They showed that the order parameter for the desorption-absorption process is the fraction of adsorbed monomers relative to the total number of monomers. As the fraction increases, more energy is required to make polymer chains stick (or detach) to a surface. Suppose that the outer layer (i.e., top layer) is composed of the loosely grafted polymer chains, as proposed by the previous studies[14, 15], the fraction of bound polymer chains would be much smaller relative to the flatten layer. As described above, the $scCO_2$ process captures the polymer chains in the stretched state even in air, reducing the fraction of polymer chains anchored to the substrate. We believe that this "screening" effect of $scCO_2$ at the polymer-substrate interface plays a crucial role in the desorption of the loosely grafted polymer chains followed by subsequent toluene washing.

4.3.4 Dynamics of the irreversibly adsorbed polymer layer.

Finally, by using NR, we have also explored the dynamics of the adsorbed layers prepared after the toluene rinsing alone under vacuum and in $scCO_2$. We first measured the interdiffusion process for a bilayer film composed of an adsorbed h-PS bottom layer (M_w = 290k, 11 nm in thickness) and a d-PS layer ($M_w = 334 \times 10^3$, 51 nm in thickness), which was overlaid on top of the h-PS adsorbed layer. The h-PS/d-PS film was annealed in a vacuum of 10^{-3} Torr at 170 ºC for 72 h. After annealing, the sample was quickly

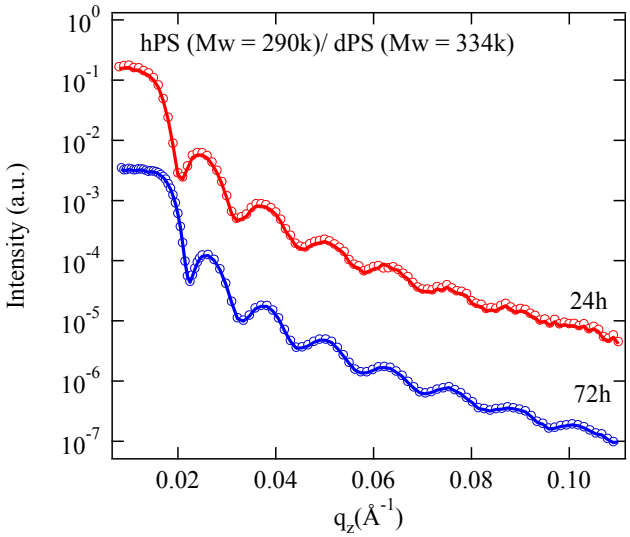

Figure 4-8. Observed (circle) and calculated (line) NR profiles of the h-PS (290 k) / d-PS (334 k) bilayer system after annealing at 170 ºC for 24 h (red) and 72 h (blue).

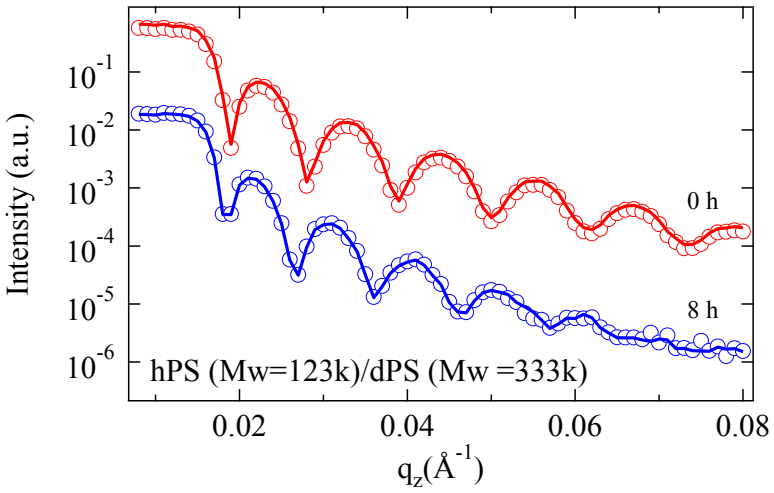

Figure 4-9. Observed (circle) and calculated (line) NR profiles of the h-PS (123 k) / d-PS (334 k) bilayer system before (red) and $scCO_2$ exposure for 8 h at the density fluctuation ridge condition (P_{ridge} = 8.2 MPa at T =36 °C)

quenched to room temperature within 2 min in air. As shown in Figure 4-8, the NR profiles remained unchanged before and after the long annealing process, giving the experimental evidence that no dynamics of the adsorbed polymer chains is favorable under vacuum even at $T>>T_g$. We then investigated the interdiffusion process of bilayer films composed of adsorbed h-PS bottom layers with different molecular weights and the same top deuterated PS layer (51 nm in thickness). We chose the density fluctuation ridge condition (P_{ridge} = 8.2 MPa at T =36 °C) for the $scCO_2$ experiments since the anomalous plasticization effect at the ridge enhances the polymer interdiffusion process by 2 orders of magnitude compared to the off-ridge conditions[30]. Figure 4-9 shows in-situ NR profiles for the bilayer of h-PS (M_w =123 $\times 10^3$)/d-PS (M_w =334 $\times 10^3$) before and after exposure to $scCO_2$ at the density fluctuation ridge. It is evident that the fringes are damped with increasing exposure time, indicating the formation of a broader interface due to the interdiffusion of the polymer chains. It should be noted that the root-mean square (rms) roughness (s) between the top d-PS and CO_2 layers was fixed to be 2 nm for the all fitting procedures[30]. From the best fits (indicated in the solid line) to the experimental data, the interfacial s value between the adsorbed h-PS and d-PS layers increases by a factor of nearly 2 (2.6 ± 0.2 nm) compared with that of the unexposed film (1.4 ± 0.2 nm). As can be seen in Figure 4-10, we find that s scales linearly with $t^{0.5}$, indicating that the diffusion between the layers progresses as Fickian diffusion[38] with a constant diffusion coefficient (D), $D = s^2/2t$. Figure 4-11 summarizes the D values as a function of M_w of the bottom adsorbed layers. For the adsorbed h-PS/d-PS bilayer systems, we see that the D scales ~ $M_w^{-3/2}$ in the range of $123\times10^3 \leq M_w \leq 2000\times10^3$, while the reptation (bulk) dynamics predicts the power of -2 instead [38]. In order to explain the deviation from the pure reptation dynamics, we introduce previous interdiffusion experiments in air for PS multilayers where a labeled layer of d-PS was placed in a

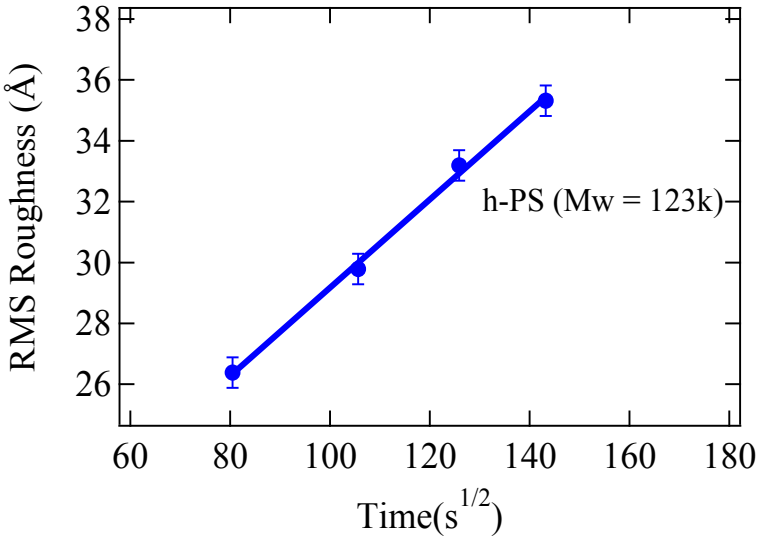

Figure 4-10. Root mean square roughness obtained from the best fits of the NR profile for the h-PS (123 k) / d-PS (334 k) bilayer system plotted as a function of exposure time.

matrix of h-PS at varying distances from the H-Si substrate interface[5, 39]. Zheng et al. have shown that the diffusion coefficient near the substrate is scaled as $N^{-3/2}$ compared to N^{-2} in the bulk. They conclude that this unusual scaling behavior can still be explained by the reptation theory considering monomer-substrate contacts (~ $N^{1/2}$ per chain) that restrict the chain mobility and modify the friction force from the bulk. Their model may be applicable here since $N^{1/2}$ contacts are characteristic of the PS adsorbed layer, as shown in Fig. 4-1. On the other hand, the D value for the bilayer composed of the h-PS (M_w=50×10^3, adsorbed layer is at least one order of magnitude smaller than that predicted from the observed relationship of $D \sim M_w^{-3/2}$. Note that the molecular weights presented are still larger than the critical entanglement molecular weight, M_c =36×10^3 for PS[40]. XR results of h-PS with $M_w < M_c$ reveal that adsorbed layer consists of only the flatten layer (~ 4 nm in thickness) even after the rinsing process with toluene. In other words, this interdiffusion takes place at the interface between the flatten layer and top d-PS overlayer, while, for the other bilayers composed of the higher M_ws adsorbed layers, the loosely grafted polymer chains mainly participate in the interdiffusion process in $scCO_2$. Hence, we can conclude that $scCO_2$ is an effective plasticizer even for such strongly adsorbed layers at the soft-hard matter interface. Moreover, it is suggestive that the polymer chains having a completely flat configuration at the interface change the conformation to a more expanded one in the direction normal to the surface due to the screening effect of $scCO_2$, promoting interdiffusion with other polymer chains which are in contact with the flat layer at the interface. Further studies on the dynamics of the flat layer are currently in progress.

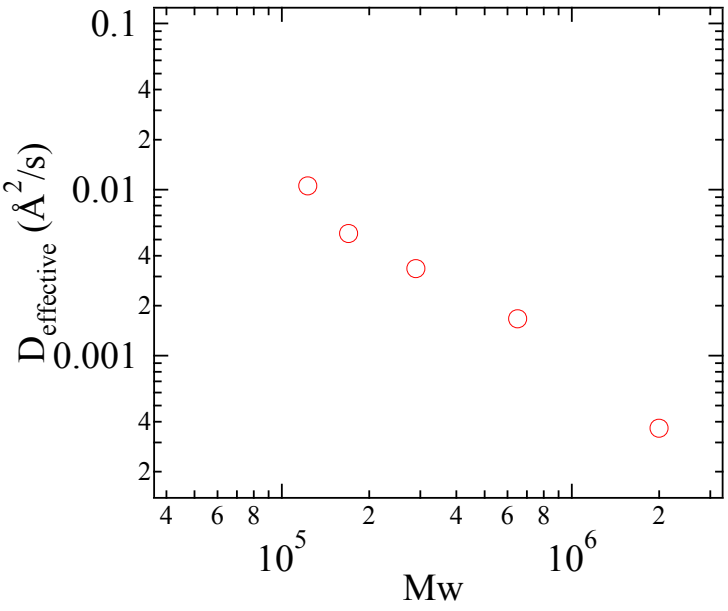

Figure 4-11. Molecular weight dependence of the diffusion coefficients obtained from the best fits of the rms roughness between the bilayer systems

4.4 Conclusions

In summary, we have revealed the formation process of PS layers adsorbed from a melt onto hydrogen-passivated silicon (H-Si) substrates. During the adsorption process, a larger (about 20%) than bulk density layer forms near the solid wall in order to make multiple contacts with the substrate, while further away from the substrate the polymer chains adsorb with the more loose, nearly random coil conformation. This difference can be explained by the fact that the inner (bottom) layer acts as an impenetrable wall for free chains to reach the solid interface, preventing strong adsorption through multiple contact points. We found that the higher density flatten layers of 3.5 ± 0.5 nm in thickness are formed regardless of the molecular weights of PS. In addition, the use of supercritical CO_2 as an effective solvent for surface modification shed new light onto the nature of the flatten layer, elucidating that the flatten conformation is thermodynamically favorable for polymer chains adsorbed at the interface. It is known that the formation of the adsorbed layer at the substrate interface is rather general and strongly affects the local property of polymer chains confined on a nanometer length scale[4]. We are currently performing further experiments for different polymers and substrates to illuminate generalities and/or differences in the formation process of the adsorbed layer. Furthermore, studies on the effects of the adsorbed layers on structures and properties at the nanoscale are also in progress, facilitating the development of new polymer nanostructures and nanodevices to be used in a wide variety of fields.

4.5 References:

[1] M. Aubouy, O. Guiselin, and E. Raphael, Macromolecules **29** (22), 7261 (1996).

[2] B. O'Shaughnessy and D. Vavylonis, Journal of Physics-Condensed Matter **17** (2), R63 (2005).

[3] S. Napolitano and M. Wubbenhorst, Nature Communications **2** (2011).

[4] T. Koga, N. Jiang, P. Gin, M. K. Endoh, S. Narayanan, L. B. Lurio, and S. K. Sinha, Physical Review Letters **107** (22), 225901 (2011).

[5] X. Zheng, B. B. Sauer, J. G. Vanalsten, S. A. Schwarz, M. H. Rafailovich, J. Sokolov, and M. Rubinstein, Physical Review Letters **74** (3), 407 (1995).

[6] S. Napolitano, C. Rotella, and M. Wubbenhorst, Macromolecular Rapid Communications **32** (11), 844 (2011).

[7] C. J. Ellison, M. K. Mundra, and J. M. Torkelson, Macromolecules **38** (5), 1767 (2005).

[8] E. K. Lin, W. I. Wu, and S. K. Satija, Macromolecules **30** (23), 7224 (1997).

[9] R. Zajac and A. Chakrabarti, Physical Review E **52** (6), 6536 (1995).

[10] P. G. Degennes, Macromolecules **14** (6), 1637 (1981).

[11] Y. Fujii, Z. H. Yang, J. Leach, H. Atarashi, K. Tanaka, and O. K. C. Tsui, Macromolecules **42** (19), 7418 (2009).

[12] C. J. Durning, B. O'Shaughnessy, U. Sawhney, D. Nguyen, J. Majewski, and G. S. Smith, Macromolecules **32** (20), 6772 (1999).

[13] A. N. Semenov, J. B. Avalos, A. Johner, and J. F. Joanny, Macromolecules **29** (6), 2179 (1996).

[14] B. O'Shaughnessy and D. Vavylonis, Physical Review Letters **90** (5) (2003).

[15] B. O'Shaughnessy and D. Vavylonis, European Physical Journal E **11** (3), 213 (2003).

[16] O. Guiselin, Europhysics Letters **17** (3), 225 (1992).

[17] H. E. Johnson and S. Granick, Science **255** (5047), 966 (1992).

[18] R. Oslanec and H. R. Brown, Macromolecules **34** (26), 9074 (2001).

[19] S. A. Sukhishvili and S. Granick, Journal of Chemical Physics **109** (16), 6861 (1998).

[20] O. H. Seeck, I. D. Kaendler, M. Tolan, K. Shin, M. H. Rafailovich, J. Sokolov, and R. Kolb, Applied Physics Letters **76** (19), 2713 (2000).

[21] T. Koga, Y. S. Seo, K. Shin, Y. Zhang, M. H. Rafailovich, J. C. Sokolov, B. Chu, and S. K. Satija, Macromolecules **36** (14), 5236 (2003).

[22] H. M. Schneider, P. Frantz, and S. Granick, Langmuir **12** (4), 994 (1996).

[23] I. Soga and S. Granick, Langmuir **14** (15), 4266 (1998).

[24] J. F. Douglas, H. E. Johnson, and S. Granick, Science **262** (5142), 2010 (1993).

[25] M. L. Fernandez, J. S. Higgins, J. Penfold, and C. S. Shackleton, Polymer Communications **31** (4), 124 (1990).

[26] W. J. Orts, J. H. Vanzanten, W. L. Wu, and S. K. Satija, Physical Review Letters **71** (6), 867 (1993).

[27] T. Miyazaki, K. Nishida, and T. Kanaya, Physical Review E **69** (6) (2004).

[28] T. Koga, Y. Ji, Y. S. Seo, C. Gordon, F. Qu, M. H. Rafailovich, J. C. Sokolov, and S. K. Satija, Journal of Polymer Science Part B-Polymer Physics **42** (17), 3282 (2004).

[29] T. Koga, P. Gin, H. Yamaguchi, M. K. Endoh, M. Asada, L. Sendogdular, M. Kobayashi, A. Takahara, B. Akgun, S. K. Satija, and T. Sumi, Polymer **52** (19), 4331 (2011).

[30] T. Koga, Y. S. Seo, X. Hu, K. Shin, Y. Zhang, M. H. Rafailovich, J. C. Sokolov, B. Chu, and S. K. Satija, Europhysics Letters **60** (4), 559 (2002).

[31] K. A. Arora, A. J. Lesser, and T. J. McCarthy, Macromolecules **31** (14), 4614 (1998).

[32] C. M. Stafford, T. P. Russell, and T. J. McCarthy, Macromolecules **32** (22), 7610 (1999).

[33] P. Gin, M. Asada, M. K. Endoh, C. Gedelian, T. M. Lu, and T. Koga, Applied Physics Letters **94** (12) (2009).

[34] K. Nishikawa, I. Tanaka, and Y. Amemiya, Journal of Physical Chemistry **100** (1), 418 (1996).

[35] T. Sato, M. Sugiyama, K. Itoh, K. Mori, T. Fukunaga, M. Misawa, T. Otomo, and S. Takata, Physical Review E **78** (5) (2008).

[36] H. M. Schneider, S. Granick, and S. Smith, Macromolecules **27** (17), 4721 (1994).

[37] S. Bhattacharya, V. G. Rostiashvili, A. Milchev, and T. A. Vilgis, Macromolecules **42** (6), 2236 (2009).

[38] M. Doi and S. F. Edwards, The Theory of Polymer Dynamics (Oxford Science, Oxford, 1986).

[39] X. Zheng, M. H. Rafailovich, J. Sokolov, Y. Strzhemechny, S. A. Schwarz, B. B. Sauer, and M. Rubinstein, Physical Review Letters **79** (2), 241 (1997).

[40] L. J. Fetters, D. J. Lohse, S. T. Milner, and W. W. Graessley, Macromolecules **32** (20), 6847 (1999).

Bibliography

Chapter I

[1] M. A. McHugh, and V. Krukonis, *Supercritical Fluids Extraction Principles and Practice* (Woburn, MA, 1994).

[2] G. Brunner, *An Introduction to Fundamentals of Supercritical Fluids and their Applications to Separation Processes* (SteinKopft Darmstadt, New York, 1994).

[3] *Supercritical Fluid Science: Fundamentals and Applications* (ACS Symp. Ser., 1993), Vol. 514.

[4] J. M. DeSimone, X. Guan, and C. S. Elsbernd, Science **257**, 945 (1992).

[5] T. Koga, Y. S. Seo, Y. Zhang, K. Shin, K. Kusano, K. Nishikawa, M. H. Rafailovich, J. C. Sokolov, B. Chu, D. Peiffer, R. Occhiogrosso, and S. K. Satija, Phys. Rev. Lett. **89**, 125506 (2002).

[6] T. Koga, Y. S. Seo, X. Hu, S. Kwanwoo, Y. Zhang, M. H. Rafailovich, J. C. Sokolov, B. Chu, and S. K. Satija, Europhys. Lett. **60**, 559 (2002).

[7] T. Koga, Y. S. Seo, K. Shin, Y. Zhang, M. Rafailovich, J. Sokolov, B. Chu, D. Peiffer, and S. K. Satija, Macromolecules **36**, 5236 (2003).

[8] T. Koga, Y. Ji, Y. S. Seo, M. H. Rafailovich, J. C. Sokolov, and S. K. Satija, J. Polym. Sci, Part B:Polym. Phys. **42**, 3282 (2004).

[9] T. Koga, Y. S. Seo, J. Jerome, S. Ge, M. H. Rafailovich, J. C. Sokolov, B. Chu, O. H. Seeck, M. Tolan, and R. Kolb, Appl. Phys. Lett. **83**, 4309 (2003).

[10] T. Koga, J. Naisheng, P. Gin, M. Endoh, S. Narayanan, L. Lurio, and S. K. Sinha, Phys. Rev. Lett. **107**, 225901 (2011).

[11] T. Koga, C. Li, M. K. Endoh, J. Koo, M. H. Rafailovich, S. Narayanan, D. R. Lee, L. Lurio, and S. K. Sinha, Phys. Rev. Lett. **104**, 066101 (2010).

[12] Y. Fujii, Z. Yang, J. Leach, H. Atarashi, K. Tanaka, and O. Tsui, Macromolecules **42**, 7418 (2009).

[13] S. C. Tucker, Chem. Rev. **99**, 391 (1999).

[14] H. E. Stanley, *Introduction to Phase Transition and Critical Phenomena* (Oxford University Press, Oxford, 1971).

[15] C. A. Eckert, D. H. Ziger, K. P. Johnston, and S. Kim, J. Phys. Chem. **90**, 2738 (1986).

[16] J. A. Gates, R. H. Wood, and J. R. Quint, J. Phys. Chem. **86**, 4948 (1982).

[17] C. A. Eckert, D. H. Ziger, K. P. Johnston, and T. K. Ellison, Fluid Phase Equilib. **14**, 167 (1983).

[18] D. B. McGuigan, and P. A. Monson, Fluid Phase Equilib. **57**, 227 (1990).

[19] E. H. Chimowitz, and G. Afrane, Fluid Phase Equilib. **120**, 167 (1996).

[20] K. S. Shing, and S. T. Chung, AIChE **34**, 1973 (1989).

[21] A. A. Chialvo, and P. T. Cummings, AIChE **40**, 1558 (1994).

[22] K. Nishikawa, I. Tanaka, and Y. Amemiya, J. Phys. Chem. **100**, 418 (1996).

[23] T. Morita, K. Kusano, H. Ochiai, K. Saitow, and K. Nishikawa, J. Chem. Phys. **112**, 4203 (2000).

[24] K. Nishikawa, and T. Morita, Chem. Phys. Lett. **316**, 238 (2000).

[25] M. Kamiya, K. Muroki, and M. Uematsu, J. Chem. Thermodyn. **27**, 337 (1995).

[26] Z. Chen, K. Tozaki, and K. Nishikawa, Jpn. J. Appl. Phys. **38**, 6840 (1999).

[27] E. F. Carome, C. B. Cykowski, J. F. havlice, and D. A. Swyt, Physica **38**, 307 (1968).

[28] C. A. Eckert, B. L. Kuntson, and P. G. Debenedetti, Nature **383**, 313 (1996).

[29] T. P. Russell, Mater. Sci. Rep. **5**, 171 (1990).

[30] G. K. Fleming, and W. J. Koros, Macromolecules **19**, 2285 (1986).

[31] R. G. Wissinger, and M. E. Paulaitis, J. Poly. Sci. Polym. Phys. Ed. **25**, 2497 (1987).

[32] J. J. Shim, and K. P. Johnston, AIChE J. **35**, 1097 (1989).

[33] B. J. Briscoe, and S. Zakaria, J. Polym. Sci. : Part B. **29**, 989 (1991).

[34] S. K. Goel, and E. J. Beckman, Polymer **34**, 1410 (1993).

[35] A. Garg, E. Gulari, and W. Manke, Macromolecules **27**, 5643 (1994).

[36] Y. Zhang, K. K. Gangwani, and R. M. Lemert, J. Supercritical Fluids **11**, 115 (1997).

[37] S. H. Chang, S. C. Park, and J. J. Shim, J. Supercritical Fluids **13**, 113 (1998).

[38] J. R. Royer, J. M. DeSimone, and S. A. Khan, Macromolecules **32**, 8965 (1999).

[39] T. Koga, J. L. Jerome, Y.-S. Seo, M. H. Rafailovich, J. C. Sokolov, and S. K. Satija, Langumuir **21**, 6157 (2005).

[40] K. A. Arora, A. J. Lesser, and T. J. McCarthy, Macromolecules **31**, 4614 (1998).

[41] C. M. Stafford, T. P. Russell, and T. J. McCarthy, Macromolecules **32**, 7610 (1999).

[42] T. Koga, E. Akashige, M. H. Rafailovich, J. C. Sokolov, K. Shin, Y. Seo, S. K. Satija, and B. Chu, Physica B **357**, 73 (2005).

[43] T. Koga, J. L. Jerome, C. Gordon, M. H. Rafailovich, and J. C. Sokolov, Journal of Adhesion **81**, 751 (2005).

[44] S. M. Sirard, Z. K. J., I. C. Sanchez, P. F. Green, and K. P. Johnston, Macromolecules **35**, 1928 (2002).

[45] Y. Li, E. Park, K. T. Lim, K. P. Johnston, and P. F. Green, J. Polym. Sci, Part B:Polym. Phys. **45**, 1313 (2007).

[46] X. Wang, and I. C. Sanchez, Langumuir **22**, 9251 (2006).

Chapter II

[1] S.C. Tucker, Chem. Rev. **99**, 391 (1999).

[2] S. Kim and K. P. Johnston, Ind. Eng. Chem. Res. **26**, 1206 (1987).

[3] H. E. Stanley, *Introduction to Phase Transition and Critical Phenomena*. (Oxford University Press, Oxford, 1971).

[4] K. Nishikawa, I. Tanaka, and Y. Amemiya, J. Phys. Chem. **100**, 418 (1996).

[5] K. Nishikawa and T. Morita, Chem. Phys. Lett. **316**, 238 (2000).

[6] Z. Chen, K. Tozaki, and K. Nishikawa, Jpn. J. Appl. Phys. **38**, 6840 (1999).

[7] E. F. Carome, C.B. Cykowski, J.F. havlice, and D.A. Swyt, Physica **38**, 307 (1968).

[8] C. A. Eckert, D. H. Ziger, K. P. Johnston, and S. Kim, J. Phys. Chem. **90**, 2738 (1986).

[9] C. A. Eckert, B. L. Kuntson, and P. G. Debenedetti, Nature **383**, 313 (1996).

[10] A. Dua and B.J. Cherayil, J. Chem. Phys. **111**, 3274 (1999).

[11] G. Luna-Barcenas, J.C. Meredith, I.C. Sanchez, K.P. Johnston, D.G. Gromov, and J.J. de Pablo, J. Chem. Phys. **107**, 10782 (1997); G. Luna-Barcenas, D.G. Gromov, J.C. Meredith, I.C. Sanchez, J.J. de Pablo, and K.P. Johnston, Chem. Phys. Lett. **278**, 302 (1997).

[12] F. Brochard and P.G. de Gennes, Ferroelectrics **30**, 33 (1980).

[13] T. Sumi and H. Sekino, J. Chem. Phys. **122**, 194910 (2005); T. Sumi, N. Imazaki, and H. Sekino, Phys. Rev. E **79**, 030801 (2009).

[14] T. Koga, Y. Ji, Y.S. Seo, M.H. Rafailovich, J.C. Sokolov, and S. K. Satija, J. Polym. Sci, Part B:Polym. Phys. **42**, 3282 (2004).

[15] T. Koga, Y.S. Seo, Y. Zhang, K. Shin, K. Kusano, K. Nishikawa, M.H. Rafailovich, J.C. Sokolov, B. Chu, D. Peiffer, R. Occhiogrosso, and S. K. Satija, Phys. Rev. Lett. **89**, 125506 (2002).

[16] T. Koga, Y.S. Seo, K. Shin, Y. Zhang, M. Rafailovich, J. Sokolov, B. Chu, D. Peiffer, and S. K. Satija, Macromolecules **36**, 5236 (2003).

[17] S. M. Sirard, Ziegler K. J., I. C. Sanchez, P. F. Green, and K.P. Johnston, Macromolecules **35**, 1928 (2002); Y. Li, E. Park, K. Lim, K.P. Johnston, and P. F. Green, J. Polym. Sci. Part B. Polym. Phys. **45**, 1313 (2007).

[18] X. Wang and I.C. Sanchez, Langmuir **22**, 9251 (2006).

[19] M.L. Anson, Adv. Protein Chem. **2**, 361 (1945).

[20] H. Yamaguchi, K. Honda, M. Kobayashi, M. Morita, H. Masunaga, O. Sakata, S. Sasaki, and A. Takahara, Polymer J. **40**, 854 (2008).

[21] C. F. Kirby and M. A. McHugh, Chem. Rev. **99**, 565 (1999).

[22] G. K. Fleming and W. J. Koros, Macromolecules **19**, 2285 (1986).

[23] E.B. Zhulina, V.A. Borisov, and T.M. Birshtein, Macromolecules **24**, 140 (1991); S. T. Milner, T. A. Witten, and M. E. Cates, Macromolecules **21**, 2160 (1988).

[24] A. Karim, S. K. Satija, J.F. Douglas, J.F. Ankner, and L. J. Fetters, Phy. Rev. Lett. **73**, 3407 (1994).

[25] T. Morita, K. Kusano, H. Ochiai, K. Saitow, and K. Nishikawa, J. Chem. Phys. **112**, 4203 (2000).

[26] B. A. Younglove and J. F. Ely, J. Phys. Chem. Ref. Data **16**, 577 (1987).

[27] F.H. Huang, M. H. Li, K. E. Starling, and F. T. H. Chung, J. Chem. Eng. Jpn. **18**, 490 (1985).

[28] T. P. Russell, Mater. Sci. Rep. **5**, 171 (1990).

[29] *The International Technology Roadmap for Semiconductors*. (2001).

[30] S. L. Xu, J. H. Lee, J. J. Kim, H. Y. Lee, and S. H. Cho, Materials Science and Engineering B-Solid State Materials for Advanced Technology **99** (1-3), 483 (2003).

Chapter III

[1] P.J. Langley and J. Hulliger, Chem. Soc. Rev. **28**, 279 (1999).

[2] A. Cooper, J. Mater. Chem. **10**, 207 (2000).

[3] L.D. Gelb, K.E. Gubbins, R. Radhakrishnan, M. Sliwinska-Bartkowiak, Rep. Prog. Phys. **62,** 1573 (1999).

[4] T. Koga, J. Jerome, M. H. Rafailovich, B. Chu, J. Douglas, and S. Satija, Adv. Coll. Interf. Sci. **128**, 217 (2006).

[5] E. Weidner, V. Wiesmet, Z. Knez, and M. Skerget, J. of Supercrit. Fluids **10**, 139 (1997).

[6] Y. Li, E. J. Park, K. T. L. Lim, K. P. Johnston, and P. F. Green, J. Polym. Sci. Part B: Polym. Phys. **45**, 1313 (2007).

[7] T. Koga, Y. S. Seo, Y. M. Zhang, K. Shin, K. Kusano, K. Nishikawa, M. H. Rafailovich, J. C. Sokolov, B. Chu, D. Peiffer, R. Occhiogrosso, and S. K. Satija, Phys. Rev. Lett. **89**, 125506 (2002).

[8] T. Koga, Y. S. Seo, K. Shin, Y. Zhang, M. H. Rafailovich, J. C. Sokolov, B. Chu, and S. K. Satija, Macromolecules **36**, 5236 (2003).

[9] T. Koga, Y. S. Seo, J. L. Jerome, S. Ge, M. H. Rafailovich, J. C. Sokolov, B. Chu, O. H. Seeck, M. Tolan, and R. Kolb, Appl. Phys. Lett. **83**, 4309 (2003).

[10] C. A. Gedelian, G. A. Ten Eyck, and T. M. Lu, Synth. Met. **157**, 48 (2007).

[11] J. Fang and E. Kiran, Macromolecules **41** (20), 7525-7535 (2008).

[12] G. Mao, J. E. Fischer, F. E. Karasz, and M. J. Winokur, J. Chem. Phys. **98**, 712 (1993).

[13] O. H. Seeck, I. D. Kaendler, M. Tolan, K. Shin, M. H. Rafailovich, J. Sokolov, and R. Kolb, Appl. Phys. Lett., **75**, 2713 (2000).

[14] K. Omote, Y. Ito, and S. Kawamura, Appl. Phys. Lett. **82**, 544 (2003).

[15] See, for example, A. Guinier and G. Fournet, *Small-Angle Scattering of X-rays* (John Wiley & Sons, London, 1955).

[16] M. Born, and E. Wolf, *In Principles of Optics*; Cambridge University Press: Cambridge, UK, 1999.

Chapter IV

[1] M. Aubouy, O. Guiselin, and E. Raphael, Macromolecules **29** (22), 7261 (1996).

[2] B. O'Shaughnessy and D. Vavylonis, Journal of Physics-Condensed Matter **17** (2), R63 (2005).

[3] S. Napolitano and M. Wubbenhorst, Nature Communications **2** (2011).

[4] T. Koga, N. Jiang, P. Gin, M. K. Endoh, S. Narayanan, L. B. Lurio, and S. K. Sinha, Physical Review Letters **107** (22), 225901 (2011).

[5] X. Zheng, B. B. Sauer, J. G. Vanalsten, S. A. Schwarz, M. H. Rafailovich, J. Sokolov, and M. Rubinstein, Physical Review Letters **74** (3), 407 (1995).

[6] S. Napolitano, C. Rotella, and M. Wubbenhorst, Macromolecular Rapid Communications **32** (11), 844 (2011).

[7] C. J. Ellison, M. K. Mundra, and J. M. Torkelson, Macromolecules **38** (5), 1767 (2005).

[8] E. K. Lin, W. I. Wu, and S. K. Satija, Macromolecules **30** (23), 7224 (1997).

[9] R. Zajac and A. Chakrabarti, Physical Review E **52** (6), 6536 (1995).

[10] P. G. Degennes, Macromolecules **14** (6), 1637 (1981).

[11] Y. Fujii, Z. H. Yang, J. Leach, H. Atarashi, K. Tanaka, and O. K. C. Tsui, Macromolecules **42** (19), 7418 (2009).

[12] C. J. Durning, B. O'Shaughnessy, U. Sawhney, D. Nguyen, J. Majewski, and G. S. Smith, Macromolecules **32** (20), 6772 (1999).

[13] A. N. Semenov, J. B. Avalos, A. Johner, and J. F. Joanny, Macromolecules **29** (6), 2179 (1996).

[14] B. O'Shaughnessy and D. Vavylonis, Physical Review Letters **90** (5) (2003).

[15] B. O'Shaughnessy and D. Vavylonis, European Physical Journal E **11** (3), 213 (2003).

[16] O. Guiselin, Europhysics Letters **17** (3), 225 (1992).

[17] H. E. Johnson and S. Granick, Science **255** (5047), 966 (1992).

[18] R. Oslanec and H. R. Brown, Macromolecules **34** (26), 9074 (2001).

[19] S. A. Sukhishvili and S. Granick, Journal of Chemical Physics **109** (16), 6861 (1998).

[20] O. H. Seeck, I. D. Kaendler, M. Tolan, K. Shin, M. H. Rafailovich, J. Sokolov, and R. Kolb, Applied Physics Letters **76** (19), 2713 (2000).

[21] T. Koga, Y. S. Seo, K. Shin, Y. Zhang, M. H. Rafailovich, J. C. Sokolov, B. Chu, and S. K. Satija, Macromolecules **36** (14), 5236 (2003).

[22] H. M. Schneider, P. Frantz, and S. Granick, Langmuir **12** (4), 994 (1996).

[23] I. Soga and S. Granick, Langmuir **14** (15), 4266 (1998).

[24] J. F. Douglas, H. E. Johnson, and S. Granick, Science **262** (5142), 2010 (1993).

[25] M. L. Fernandez, J. S. Higgins, J. Penfold, and C. S. Shackleton, Polymer Communications **31** (4), 124 (1990).

[26] W. J. Orts, J. H. Vanzanten, W. L. Wu, and S. K. Satija, Physical Review Letters **71** (6), 867 (1993).

[27] T. Miyazaki, K. Nishida, and T. Kanaya, Physical Review E **69** (6) (2004).

[28] T. Koga, Y. Ji, Y. S. Seo, C. Gordon, F. Qu, M. H. Rafailovich, J. C. Sokolov, and S. K. Satija, Journal of Polymer Science Part B-Polymer Physics **42** (17), 3282 (2004).

[29] T. Koga, P. Gin, H. Yamaguchi, M. K. Endoh, M. Asada, L. Sendogdular, M. Kobayashi, A. Takahara, B. Akgun, S. K. Satija, and T. Sumi, Polymer **52** (19), 4331 (2011).

[30] T. Koga, Y. S. Seo, X. Hu, K. Shin, Y. Zhang, M. H. Rafailovich, J. C. Sokolov, B. Chu, and S. K. Satija, Europhysics Letters **60** (4), 559 (2002).

[31] K. A. Arora, A. J. Lesser, and T. J. McCarthy, Macromolecules **31** (14), 4614 (1998).

[32] C. M. Stafford, T. P. Russell, and T. J. McCarthy, Macromolecules **32** (22), 7610 (1999).

[33] P. Gin, M. Asada, M. K. Endoh, C. Gedelian, T. M. Lu, and T. Koga, Applied Physics Letters **94** (12) (2009).

[34] K. Nishikawa, I. Tanaka, and Y. Amemiya, Journal of Physical Chemistry **100** (1), 418 (1996).

[35] T. Sato, M. Sugiyama, K. Itoh, K. Mori, T. Fukunaga, M. Misawa, T. Otomo, and S. Takata, Physical Review E **78** (5) (2008).

[36] H. M. Schneider, S. Granick, and S. Smith, Macromolecules **27** (17), 4721 (1994).

[37] S. Bhattacharya, V. G. Rostiashvili, A. Milchev, and T. A. Vilgis, Macromolecules **42** (6), 2236 (2009).

[38] M. Doi and S. F. Edwards, The Theory of Polymer Dynamics (Oxford Science, Oxford, 1986).

[39] X. Zheng, M. H. Rafailovich, J. Sokolov, Y. Strzhemechny, S. A. Schwarz, B. B. Sauer, and M.

Rubinstein, Physical Review Letters **79** (2), 241 (1997).

[40] L. J. Fetters, D. J. Lohse, S. T. Milner, and W. W. Graessley, Macromolecules **32** (20), 6847 (1999).